ESAIM: PROCEEDINGS AND SURVEYS, August 2023, Vol. 72, p. 93-116
Philippe Helluy, Jean-Marc Hérard, Nicolas Seguin

AN ACOUSTIC-TRANSPORT SPLITTING METHOD FOR THE BAROTROPIC BAER-NUNZIATO TWO-PHASE FLOW MODEL *

Katia Ait-Ameur[1], Samuel Kokh[2], Marc Massot[1], Marica Pelanti[3] and Teddy Pichard[1]

Abstract. This work focuses on the numerical approximation of the barotropic Baer-Nunziato two-phase flow model. We propose a numerical scheme that relies on an operator splitting method corresponding to a separate treatment of the acoustic and the material transport phenomena. In the subsonic case, this also corresponds to a separate treatment of the fast and the slow propagation phenomena. This approach follows the lines of the implicit-explicit schemes developed in [8]. The operator splitting enable the use of time steps that are no longer constrained by the sound velocity thanks to an implicit treatment of the acoustic waves, while maintaining accuracy in the subsonic regime thanks to an explicit treatment of the material waves. In the present setting, a particular attention will be also given to the discretization of the non-conservative terms that figure in the two-phase model. We prove that the proposed numerical strategy is positivity preserving for the volume fractions and the partial masses. The scheme is tested against several one-dimensional test cases including flows featuring vanishing phases.

Résumé. Ce travail porte sur l'approximation numérique du modèle de Baer-Nunziato barotrope. Le schéma se base sur une méthode de splitting correspondant à un traitement séparé des ondes acoustiques d'une part et des ondes matières d'autre part. Nous proposons d'étendre les schémas implicites-explicites développés dans [8]. Ces méthodes permettent d'utiliser des pas de temps qui ne sont plus contraints par la vitesse du son grâce à un traitement implicite des ondes acoustiques, et de conserver une précision dans le régime subsonique grâce à un traitement explicite des ondes matières. Dans ce travail, une attention particulière sera également portée à la discrétisation des termes non conservatifs dans le modèle de Baer-Nunziato. Nous montrons que les méthodes numériques proposées préservent la positivité des densités et des fractions volumiques et nous illustrons leurs comportements à l'aide de plusieurs cas tests représentatifs des difficultés numériques liées à ce modèle.

1. Introduction

We are interested in the computation of compressible two-phase flows with a two-velocity two-pressure model derived after the Baer-Nunziato (BN) model [3]. The (BN) model was initially dedicated to modeling a gas-solid flow for the simulation of detonation phenomena [3]. Its range of applications has since been extended to a wider

* *This work was supported by a grant from Region Ile-de-France DIM MATHINNOV and the DGA project MMEED.*

[1] CMAP, CNRS, École polytechnique, Institut Polytechnique de Paris, 91120 Palaiseau, France; e-mail: `katia.ait-ameur@polytechnique.edu, marc.massot@polytechnique.edu, teddy.pichard@polytechnique.edu`

[2] Université Paris-Saclay, CEA, Service de Génie Logiciel pour la Simulation, 91191, Gif-sur-Yvette, France; e-mail: `samuel.kokh@cea.fr`

[3] IMSIA, ENSTA Paris - EDF - CNRS - CEA, Institut Polytechnique de Paris, 828, Boulevard des Maréchaux, Palaiseau, 91120, France; e-mail: `marica.pelanti@ensta-paris.fr`

Article published online by EDP Sciences and available at https://www.esaim-proc.org or https://doi.org/10.1051/proc/202372093

range of two-material flows like liquid-gas flows (see for example [11, 14, 18, 20, 22, 23, 25]). In the present work, we adopt a simplified version of the (BN) model that involves only mass and momentum equations equipped with a barotropic pressure law (as in [15, 16]): the pressure p_k of each component $k = 1, 2$ is assumed to only depend on the phasic density ρ_k. A specific feature of this model that is inherited from the full (BN) model lies in the presence of non-conservative terms that drive the coupling between both fluids. These terms involve so-called interfacial velocity and interfacial pressure. The definition of these parameters require additional closure relations. This choice is not straightforward and has important consequences on the mathematical properties of the model, like the ability to define weak-solutions or to equip the model with an entropy evolution equation (see for example [19]).

From a numerical point of view, the barotropic (BN) model raises several issues. A first difficulty comes from the presence of non-conservative terms and how they may interact with conservative fluxes. A second difficulty occurs when the volume fraction of one of the component tends to zero in some regions of the computational domain. This situation is referred to as a vanishing phase and may cause severe problem as numerical methods often fail to compute the phasic quantities associated with the vanishing phase [15].

One may find in the literature several papers devoted to the numerical resolution of two-fluid two-pressure models and the question of how to discretize the non conservative terms. Most of them deal with the non barotropic case. The reader is referred to [1, 2, 26, 29] for the numerical methods relying on time-explicit, exact or approximate Riemann solver and the references therein. We also mention some other finite volume techniques that have been used. In [19], the authors extend Rusanov's scheme and the VFRoe method to the context of non conservative systems. Other schemes rely on relaxation techniques (see for instance [1, 15]).

The discretization of the full (BN) model has been investigated by many authors in the literature (see for example [1,6,14–16,19,25,26,29]) but in most contributions, for stability reasons, the time steps Δt is subject to a CFL condition that depends on the material velocity and the sound velocity of each material. For configurations where the sound velocities are much larger than the material velocities, this can lead to very small time steps although the acoustic waves are not driving phenomena in the flow. A CFL condition based on the most influent waves, the contact waves associated to the material velocities would be more adapted. The idea is then to propose a time-implicit treatment of the acoustic waves, in order to get rid of a too restrictive CFL condition, together with an explicit treatment of the contact waves in order to preserve accuracy. This strategy has already been exploited earlier within the framework of Euler equations and Shallow Water equations (see for instance [8,10,17]) using a Lagrange-Projection approach, but also for two-phase flows models (see [6, 9, 16, 24, 28, 30]).

The paper is organized as follows. In Section 2, we present the set of partial differential equations (PDEs) of barotropic (BN) model, and we recall its main mathematical properties. In Section 3, we propose an operator splitting method for approximating the solutions of the model. In Section 4, we describe the numerical treatment of each step. In Section 5, we build explicit and semi-implicit numerical schemes based on this operator splitting method for the solution of the barotropic (BN) model. Finally, Section 6 is devoted to the numerical experiments, where one-dimensional test cases are presented.

2. The barotropic Baer-Nunziato model

Let us consider two compressible materials $k = 1, 2$, equipped with a barotropic Equation Of State (EOS) of the form $\rho_k \mapsto e_k(\rho_k)$, where e_k and ρ_k respectively denote the specific barotropic potential energy and density of the fluid k. The pressure p_k is defined by $p_k(\rho_k) = \rho_k^2 \mathrm{d}e_k/\mathrm{d}\rho_k$. We assume the sound velocity c_k of the fluid k to be real-valued and defined by $c_k^2 = p_k'(\rho_k) > 0$.

We denote α_k the volume fraction associated with the component k and impose that $\alpha_1 + \alpha_2 = 1$. If u_k is the velocity of the fluid $k = 1, 2$, for one-dimensional problems the barotropic BN model reads:

$$\left\{\begin{array}{lcll} \partial_t \alpha_1 & + & u_I \partial_x \alpha_1 & = 0, \\ \partial_t(\alpha_1\rho_1) & + & \partial_x(\alpha_1\rho_1 u_1) & = 0, \\ \partial_t(\alpha_1\rho_1 u_1) & + & \partial_x(\alpha_1\rho_1 u_1^2 + \alpha_1 p_1) - p_I \partial_x \alpha_1 & = 0, \\ \partial_t(\alpha_2\rho_2) & + & \partial_x(\alpha_2\rho_2 u_2) & = 0, \\ \partial_t(\alpha_2\rho_2 u_2) & + & \partial_x(\alpha_2\rho_2 u_2^2 + \alpha_2 p_2) - p_I \partial_x \alpha_2 & = 0, \end{array}\right. \tag{1}$$

where u_I and p_I are the interfacial velocity and pressure for which one must provide closure laws. This system involves two evolution equations for both the partial mass and momentum of the fluid $k = 1, 2$ supplemented by an equation for the volume fraction $\alpha_1 = 1 - \alpha_2$.

The eigenstructure of (1) consists of five real eigenvalues

$$Sp = \{u_I, u_1 \pm c_1, u_2 \pm c_2, \}.$$

The barotropic BN model is hyperbolic under the following conditions:

$$\alpha_1\alpha_2 \neq 0, \quad |u_k - u_I| \neq c_k, \quad k = 1, 2.$$

When (1) is hyperbolic, one can easily check that similarly to the classical gas dynamics equations, the characteristic fields associated with the eigenvalues $u_k \pm c_k$ are genuinely nonlinear.

The choice of the closure law for u_I has an important impact on the evolution of α_k as it may not be possible to obtain a maximum principle for α_k if the field associated with u_I is not linearly degenerate. Moreover, the choice of both u_I and p_I affects the availability of weak solutions and a companion entropy evolution equation for the system. For these reasons, as in [15, 16] we restrict our study to the following closure relations

$$\begin{array}{lcl} u_I & = & (1-\mu)u_1 + \mu u_2, \quad \mu = \frac{\chi\alpha_1\rho_1}{\chi\alpha_1\rho_1 + (1-\chi)\alpha_2\rho_2}, \quad \chi \in \left\{0, \frac{1}{2}, 1\right\}, \\ p_I & = & \mu p_1 + (1-\mu)p_2, \end{array} \tag{2}$$

that issued from [12, 19]. This choice ensures that the field associated with u_I is linearly degenerate, it also provides a complete set of jump relations that enables a full definition of weak solutions and an entropy evolution equation. As a consequence, smooth solutions of (1) with (2) also verify the following conservation equation

$$\partial_t \left\{ \sum_{k=1}^{2} \alpha_k\rho_k e_k(\rho_k) + \alpha_k\rho_k \frac{u_k^2}{2} \right\} + \partial_x \left\{ \sum_{k=1}^{2} \alpha_k\rho_k e_k(\rho_k)u_k + \alpha_k\rho_k \frac{u_k^3}{2} + \alpha_k p_k(\rho_k)u_k \right\} = 0. \tag{3}$$

Let us underline that for the numerical results presented in the last section, we will restrict our choice to the case $\chi = 0, \mu = 1$ so that

$$(u_I, p_I) = (u_2, p_1). \tag{4}$$

Finally, we denote $\mathbb{U} = (\alpha_1, \alpha_1\rho_1, \alpha_1\rho_1 u_1, \alpha_2\rho_2, \alpha_2\rho_2 u_2)$ the unknown vector that is expected to belong to the set of admissible states:

$$\Omega = \left\{\mathbb{U} \in \mathbb{R}^5, \quad 0 < \alpha_k < 1, \quad \rho_k > 0, \quad k \in \{1, 2\}, \quad \alpha_1 + \alpha_2 = 1\right\}. \tag{5}$$

System (1) takes the following condensed form

$$\partial_t \mathbb{U} + \partial_x F(\mathbb{U}) + C(\mathbb{U})\partial_x \mathbb{U} = 0, \quad x \in \mathbb{R}, \quad t > 0, \tag{6}$$

where

$$F(\mathbb{U}) = \begin{pmatrix} 0 \\ \alpha_1\rho_1 u_1 \\ \alpha_1\rho_1 u_1^2 + \alpha_1 p_1(\rho_1) \\ \alpha_2\rho_2 u_2 \\ \alpha_2\rho_2 u_2^2 + \alpha_2 p_2(\rho_2) \end{pmatrix}, \quad C(\mathbb{U})\partial_x\mathbb{U} = \begin{pmatrix} u_I\partial_x\alpha_1 \\ 0 \\ -p_I\partial_x\alpha_1 \\ 0 \\ -p_I\partial_x\alpha_2 \end{pmatrix}. \tag{7}$$

3. Operator splitting acoustic-transport

Before going further on, we recall that this idea has already been used earlier within the framework of Euler equations (see for instance [17]) using a Lagrange-Projection approach, but also for the Baer-Nunziato model (see [6,16]). In [6], the authors propose an operator splitting with three steps for the Baer Nunziato model with energy equations. Both first steps correspond to the acoustic and transport parts of the Euler equations for each phase. The third step gathers the non conservative terms that couple both phases. In [16], the authors propose an operator splitting in two steps where the coupling terms are distributed in the two subsytems. In this case, the transport part arises a weakly hyperbolic system and a careful treatment has to be made for the numerical discretization. In this section, we introduce an operator splitting for the barotropic BN model in two steps where the two subsystems account for the coupling terms like [16] while preserving the hyperbolicity of each subsystem as in [6].

The first step corresponds to the propagation of acoustic waves:

$$\left\{ \begin{array}{lcll} \partial_t\alpha_1 & & = & 0, \\ \partial_t(\alpha_k\rho_k) + (\alpha_k\rho_k)\partial_x u_k & & = & 0, \quad k \in \{1,2\}, \\ \partial_t(\alpha_k\rho_k u_k) + (\alpha_k\rho_k u_k)\partial_x u_k + \partial_x(\alpha_k p_k) - p_I\partial_x\alpha_k & & = & 0, \quad k \in \{1,2\}. \end{array} \right. \tag{8}$$

The second step considers the propagation of both material waves and the evolution of α_k:

$$\left\{ \begin{array}{lcll} \partial_t\alpha_1 + u_I\partial_x\alpha_1 & & = & 0, \\ \partial_t(\alpha_k\rho_k) + u_k\partial_x\alpha_k\rho_k & & = & 0, \quad k \in \{1,2\}, \\ \partial_t(\alpha_k\rho_k u_k) + u_k\partial_x(\alpha_k\rho_k u_k) & & = & 0, \quad k \in \{1,2\}. \end{array} \right. \tag{9}$$

3.1. Properties of the acoustic sub-system

If we note $\tau_k = \rho_k^{-1}$ the specific volume, the acoustic system (8) takes the form

$$\left\{ \begin{array}{lcll} \partial_t\alpha_1 & & = & 0, \\ \rho_k\partial_t\tau_k - \partial_x u_k & & = & 0, \\ \rho_k\partial_t(\alpha_k u_k) + \partial_x(\alpha_k p_k) - p_I\partial_x\alpha_k & & = & 0. \end{array} \right. \tag{10}$$

Granted that $c_1 \neq c_2$, the acoustic system (10) is strictly hyperbolic and the eigenstructure of the system is composed of five fields associated with the eigenvalues $\{\pm c_1, 0, \pm c_2\}$. The waves associated with $\pm c_k$ are genuinely nonlinear. The wave associated with 0 is linearly degenerate.

We propose further approximations for the acoustic system (8) by freezing the time dependence of ρ_k in front of $\rho_k\partial_t(\cdot)$ in (10) and by using a Suliciu-type relaxation approximation of (10) (see [7,13,27]). We proceed by introducing new independent variables π_k and r_k that respectively act as surrogate pressure and densities for $k = 1, 2$. If one considers smooth solutions of (8), the pressure p_k verifies

$$\rho_k\partial_t(\alpha_k p_k) + \alpha_k(c_k/\tau_k)^2\partial_x u_k = 0. \tag{11}$$

The variables π_k are evolved according to their own partial differential equations, whose purpose is to implement a linearized version of (11). The new variables r_k are associated with a stationary wave. Therefore, within the time interval $t \in [t^n, t^n + \Delta t[$, we propose to consider the following relaxation system

$$\left\{\begin{array}{lcll} \partial_t \alpha_1 & & = & 0, \\ \partial_t r_k & & = & \nu\left(\rho_k - r_k\right), \\ \partial_t (r_k \tau_k) & - \partial_x u_k & = & 0, \\ \partial_t (r_k \alpha_k u_k) & + \partial_x (\alpha_k \pi_k) & = & \pi_I \partial_x \alpha_k, \\ \partial_t (r_k \pi_k) & + a_k^2 \partial_x u_k & = & \nu\left(p_k - \pi_k\right) r_k, \end{array}\right. \tag{12}$$

where ν is a relaxation parameter and a_k is a constant approximation of the acoustic impedance of the fluid k. In the limit regime $\nu \to \infty$, we formally retrieve the solution of (8). In order to provide a stable approximation of (8), the constants a_k must be chosen in agreement with the Whitham subcharacteristic condition

$$a_k^2 > \max_{\rho_k} \left(\rho_k^2 c_k^2(\rho_k)\right), \quad k = 1, 2, \tag{13}$$

where the max is taken over all the density values ρ_k in the solution of (12). We adopt the classic method that allows to reach the regime $\nu \to \infty$: at each time step, we enforce the equilibrium relations $(\pi_k)_j^n = p_k^{EOS}((\rho_k)_j^n)$, $(r_k)_j^n = (\rho_k)_j^n$ and solve (12) with $\nu = 0$.
For $\nu = 0$, the relaxation system can take the compact form:

$$\left\{\begin{array}{ll} \partial_t \alpha_1 & = 0, \\ \partial_t \mathbb{W}_k + \partial_x G_k(\mathbb{W}_k) & = \left(\pi_I \partial_x \alpha_k\right) E, \quad k \in \{1, 2\}, \end{array}\right. \tag{14}$$

with the unknown $\mathbb{W}_k = (r_k, r_k\tau_k, r_k\alpha_k u_k, r_k \pi_k)$, the flux $G_k(\mathbb{W}_k) = \left(0, -u_k, \alpha_k \pi_k, a_k^2 u_k\right)$ and $E = (0, 0, 1, 0)$. Let us discuss a few properties of (14). Straightforward computations (see Appendix A) provide the following property on the characteristic fields of the relaxation system.

Proposition 3.1. *For any state vector $(\alpha_1, \mathbb{W}_1, \mathbb{W}_2)$, system (14) has the following characteristic speeds:*

$$Sp = \left\{\pm \frac{a_1}{r_1}, 0, \pm \frac{a_2}{r_2}\right\},$$

where 0 is of multiplicity five. Moreover, all the characteristic fields are linearly degenerate and system (14) is hyperbolic.

3.2. **Properties of the transport sub-system**

We now consider the time evolution corresponding to the transport step. Starting from the output of the first step $\mathbb{U}^\sharp$, we want to compute the updated data $\mathbb{U}^{n+1}$ at time t^{n+1} by approximating the solution of

$$\left\{\begin{array}{lcll} \partial_t \alpha_1 & + u_I \partial_x \alpha_1 & = & 0, \\ \partial_t (\alpha_k \rho_k) & + u_k \partial_x (\alpha_k \rho_k) & = & 0, \quad k \in \{1, 2\}, \\ \partial_t (\alpha_k \rho_k u_k) & + u_k \partial_x (\alpha_k \rho_k u_k) & = & 0, \quad k \in \{1, 2\}. \end{array}\right.$$

The eigenstructure of (9) is derived thanks to straightforward computations.

Proposition 3.2. *For any state vector $(\alpha_1, \alpha_1\rho_1, \alpha_1\rho_1 u_1, \alpha_2\rho_2, \alpha_2\rho_2 u_2)$ such that $\rho_1 > 0$ and $\rho_2 > 0$, system (9) has the following characteristic speeds:*

$$Sp = \{u_I, u_1, u_2\}.$$

Assuming that the interfacial velocity u_I is defined by the closure law (2) then the characteristic field associated to the (simple) eigenvalue u_I is linearly degenerate. The characteristic fields associated to the (double) eigenvalues u_k are genuinely non linear and system (9) is weakly hyperbolic.

Remark 3.3. Let us emphasize that the nature of the characteristic field associated with the eigenvalue u_I in (9) depends on the chosen closure law for u_I in the complete model (1). For example, assuming a different closure law as in [21] by setting:

$$u_I = \alpha_1 u_1 + \alpha_2 u_2,$$

would lead to a genuinely non linear characteristic field associated to the eigenvalue u_I in both (1) and (9).

Remark 3.4. The transport system (9) shares a similar structure with the system of pressureless gases (see for example [4, 5]). However, in our case, its sole purpose is to yield a discretization means for the transport terms of the barotropic BN model (1). Let us underline that in the discretization strategy presented in Section 4.2, the propagation velocities (9) will be frozen at values $u_I^\star$ and $u_k^\star$ computed at the acoustic step. This will enable a discretization of (9) that verifies a local maximum principle for α_k, $\alpha_k\rho_k$ and $\alpha_k\rho_k u_k$. Moreover, the overall discretization is consistent with the barotropic BN model (1). In this sense, possible well-posedness issues involved with the transport system (9) are not a genuine concern here and will not be investigated.

4. Discretization of the acoustic and transport sub-systems

In this section, we use the operator splitting method in order to derive an implicit-explicit numerical scheme, the aim being to approximate the solutions of the barotropic BN model (6). Let Δt be the time step and Δx the space step, which we assume here to be constant for simplicity in the notations. The space is partitioned into cells $C_j = [x_{j-\frac{1}{2}}, x_{j+\frac{1}{2}}]$, $\quad j \in \mathbb{Z}$ where $x_{j+\frac{1}{2}} = (j+\frac{1}{2})\Delta x$ are the cell interfaces. At the discrete times $t^n = n\Delta t$, the cell average of the solution of (6) is approximated on each cell C_j by a constant value denoted by

$$\mathbb{U}_j^n = \left((\alpha_1)_j^n, (\alpha_1\rho_1)_j^n, (\alpha_1\rho_1 u_1)_j^n, (\alpha_2\rho_2)_j^n, (\alpha_2\rho_2 u_2)_j^n\right).$$

In the following two sections, we describe the discretization strategy associated with the operator splitting method in order to calculate the values $\left(\mathbb{U}_j^{n+1}\right)_{j\in\mathbb{Z}}$ of the approximate solution at time t^{n+1} from those at time t^n. Section 4.1 displays the numerical treatment of the Lagrangian step (8) while section 4.2 deals with the material transport step (9).

4.1. Treatment of the first step

We need to propose a discretization strategy for (14). The solution of a Riemann problem for (14) consists in six constant states separated by five contact discontinuities. We choose to build an approximate Riemann solver for the relaxation acoustic system (14). We will use in the sequel a discretization of the non conservative product that is consistent with the term $\pi_I \partial_x \alpha_k$ to derive an approximate Riemann solver for (14). Let $\Delta x_L > 0, \Delta x_R > 0$. We consider a piecewise initial data defined by:

$$\begin{array}{rcl} \alpha_1(x, t=0) & = & \left\{ \begin{array}{ll} (\alpha_1)_L, & \text{if } x \le 0, \\ (\alpha_1)_R, & \text{if } x > 0, \end{array} \right. \\ \mathbb{W}_k(x, t=0) & = & \left\{ \begin{array}{ll} (\mathbb{W}_k)_L = \left((r_k)_L, (r_k\tau_k)_L, (r_k\alpha_k u_k)_L, (r_k\pi_k)_L\right), & \text{if } x \le 0, \\ (\mathbb{W}_k)_R = \left((r_k)_R, (r_k\tau_k)_R, (r_k\alpha_k u_k)_R, (r_k\pi_k)_R\right), & \text{if } x > 0, \end{array} \right. \end{array} \tag{15}$$

where the left and right states are defined by:

$$(\pi_k)_L = p_k^{EOS}((\tau_k)_L), \quad (\pi_k)_R = p_k^{EOS}((\tau_k)_R), \quad (r_k)_L = (\rho_k)_L, \quad (r_k)_R = (\rho_k)_R.$$

Note that $(\pi_k)_L$, $(\pi_k)_R$, $(r_k)_L$ and $(r_k)_R$ are at equilibrium. Let us now build an approximate Riemann solver for the relaxed acoustic system (14). We look for a function $(\mathbb{W}_k)_{RP}$ composed of six states separated by

discontinuities as follows:

$$(\mathbb{W}_k)_{RP}\left(\frac{x}{t};(\mathbb{W}_k)_L,(\mathbb{W}_k)_R\right)=\begin{cases}(\mathbb{W}_k)_L & \text{if} \quad \frac{x}{t}<-\frac{a_k}{(r_k)_L},\\ (\mathbb{W}_k)^\star_L & \text{if} \quad -\frac{a_k}{(r_k)_L}<\frac{x}{t}<0,\\ (\mathbb{W}_k)^\star_R & \text{if} \quad 0<\frac{x}{t}<\frac{a_k}{(r_k)_R},\\ (\mathbb{W}_k)_R & \text{if} \quad \frac{x}{t}>\frac{a_k}{(r_k)_R}.\end{cases} \tag{16}$$

The function $(\alpha_1)_{RP}$ is defined as follows:

$$(\alpha_1)_{RP}\left(\frac{x}{t};(\alpha_1)_L,(\alpha_1)_R\right)=\begin{cases}(\alpha_1)_L & \text{if} \quad \frac{x}{t}<0,\\ (\alpha_1)_R & \text{if} \quad \frac{x}{t}>0.\end{cases} \tag{17}$$

The intermediate states in (16) are such that the following properties hold:

(1) $(\mathbb{W}_k)_{RP}$ is consistent in the integral sense with the barotropic Baer Nunziato model. More specifically in our context, if Δt is such that $\frac{a_k}{(r_k)_R}\Delta t\leq \min(\Delta x_L,\Delta x_R)/2$, then

$$\begin{array}{rcl} G_k((\mathbb{W}_k)_R)-G_k((\mathbb{W}_k)_L)= & - & \dfrac{a_k}{(r_k)_L}\left((\mathbb{W}_k)^\star_L-(\mathbb{W}_k)_L\right)+\dfrac{a_k}{(r_k)_R}\left((\mathbb{W}_k)_R-(\mathbb{W}_k)^\star_R\right)\\ & - & \dfrac{\Delta x_L+\Delta x_R}{2}\left\{\pi_I\partial_x\alpha_k\right\}E,\end{array} \tag{18}$$

where $\{\pi_I\partial_x\alpha_k\}$ is consistent with the non conservative term, in the sense:

$$\lim_{\substack{\Delta x_L,\,\Delta x_R\to 0,\\ (\mathbb{W}_k)_L,\,(\mathbb{W}_k)_R\to(\overline{\alpha_k},\overline{\tau_k},\overline{u_k},\overline{\pi_k})}}\left\{\pi_I\partial_x\alpha_k\right\}=\overline{\pi_I}(\partial_x\alpha_k)(\overline{\alpha_k}). \tag{19}$$

(2) We impose that $(\mathbb{W}_k)_L$ and $(\mathbb{W}_k)^\star_L$ (resp. $(\mathbb{W}_k)_R$ and $(\mathbb{W}_k)^\star_R$) verify the Rankine Hugoniot jump conditions accross $\left(-\frac{a_k}{(r_k)_L}\right)$-wave (resp. $\left(\frac{a_k}{(r_k)_R}\right)$-wave):

$$\begin{array}{rcl} \frac{a_k}{(r_k)_L}\left((\mathbb{W}_k)^\star_L-(\mathbb{W}_k)_L\right) & + & G_k((\mathbb{W}_k)^\star_L)-G_k((\mathbb{W}_k)_L) \;=\; 0,\\ -\frac{a_k}{(r_k)_R}\left((\mathbb{W}_k)_R-(\mathbb{W}_k)^\star_R\right) & + & G_k((\mathbb{W}_k)_R)-G_k((\mathbb{W}_k)^\star_R) \;=\; 0.\end{array} \tag{20}$$

(3) Similarly, across the discontinuity of velocity 0 we impose that:

$$(u_k)^\star_L=(u_k)^\star_R=(u_k)^\star,\quad (\alpha_1\pi_1)^\star_L+(\alpha_2\pi_2)^\star_L=(\alpha_1\pi_1)^\star_R+(\alpha_2\pi_2)^\star_R. \tag{21}$$

Relations (20) and (21) do not provide enough information to determine the intermediate states $(\mathbb{W}_k)^\star_L$ and $(\mathbb{W}_k)^\star_R$. Indeed, they provide only seven independent relations while we need eight quantities, namely $(u_k)^\star_L$, $(u_k)^\star_R$, $(\alpha_k\pi_k)^\star_L$ and $(\alpha_k\pi_k)^\star_R$.

We choose to add another jump relation accross the stationary discontinuity of $(\mathbb{W}_k)_{RP}$, we impose

$$(\alpha_k\pi_k)^\star_R-(\alpha_k\pi_k)^\star_L=\mathcal{M}_k, \tag{22}$$

where $\mathcal{M}_k$ is a function to be specified. Relations (18), (20), (21) and (22) lead to:

$$\begin{cases} \overline{\alpha_k}u^\star_k & = & \overline{\alpha_k u_k}-\dfrac{1}{2a_k}\Delta(\alpha_k\pi_k)+\dfrac{\mathcal{M}_k}{2a_k},\\ \pi^\star_k & = & \overline{\pi_k}-\frac{a_k}{2}\Delta u_k,\\ \overline{\alpha_k}(\pi_k)^\star_L & = & (\alpha_k)_R\pi^\star_k-\frac{\mathcal{M}_k}{2},\\ \overline{\alpha_k}(\pi_k)^\star_R & = & (\alpha_k)_L\pi^\star_k+\frac{\mathcal{M}_k}{2}.\end{cases} \tag{23}$$

We now only need to determine $\mathcal{M}_k$ such that the conditions 1), 2) and 3) are satisfied. The integral consistency requirement of Condition 1) imposes

$$\mathcal{M}_k = \{\pi_I \partial_x \alpha_k\} \frac{\Delta x_L + \Delta x_R}{2}. \tag{24}$$

A simple mean to comply with (24) is to choose:

$$\mathcal{M}_k = \pi_I^{\Delta}((\mathbb{W}_k)_L, (\mathbb{W}_k)_R) \left[(\alpha_k)_R - (\alpha_k)_L\right],$$

where $\pi_I^{\Delta}((\mathbb{W}_k)_L, (\mathbb{W}_k)_R)$ is a consistent approximation of π_I in the sense that:

$$\pi_I^{\Delta}((\mathbb{W}_k)_L, (\mathbb{W}_k)_R) \to \overline{\pi_I} \qquad \text{if} \qquad (\pi_I)_L, (\pi_I)_R \to \overline{\pi_I}.$$

At last, we choose:

$$\pi_I^{\Delta}((\mathbb{W}_k)_L, (\mathbb{W}_k)_R) = \pi_1^{\star} = \frac{\pi_1^L + \pi_1^R}{2} - a_1 \frac{\pi_1^R - \pi_1^L}{2}. \tag{25}$$

This yields that

$$\{\pi_I \partial_x \alpha_k\}((\mathbb{W}_k)_L, (\mathbb{W}_k)_R, \Delta x_L, \Delta x_R) = 2\pi_I^{\Delta}((\mathbb{W}_k)_L, (\mathbb{W}_k)_R) \frac{(\alpha_k)_R - (\alpha_k)_L}{\Delta x_L + \Delta x_R}. \tag{26}$$

By construction, the approximate Riemann solver defined by (23) and (26) verifies the three conditions 1), 2) and 3). We end up with the following update at the acoustic step:

$$\left\{\begin{array}{rcl}
(\alpha_1)_j^{\sharp} &=& (\alpha_1)_j^n, \\
(r_k)_j^{\sharp} &=& (r_k)_j^n, \\
(\tau_k)_j^{\sharp} &=& (\tau_k)_j^n + \frac{\Delta t}{\Delta x (r_k)_j^n}\left((u_k)_{j+1/2}^{\star} - (u_k)_{j-1/2}^{\star}\right), \\
(u_k)_j^{\sharp} &=& (u_k)_j^n - \frac{\Delta t}{\Delta x (\alpha_k r_k)_j^n}\left((\alpha_k \pi_k)_{j+1/2}^{\star} - (\alpha_k \pi_k)_{j-1/2}^{\star}\right) + \frac{\Delta t}{(\alpha_k r_k)_j^n}\left\{\pi_I \partial_x \alpha_k\right\}_j^n, \\
(\pi_k)_j^{\sharp} &=& (\pi_k)_j^n - \frac{\Delta t}{\Delta x (r_k)_j^n} a_k^2 \left((u_k)_{j+1/2}^{\star} - (u_k)_{j-1/2}^{\star}\right),
\end{array}\right. \tag{27}$$

where $(\pi_k)_j^n = p_k^{EOS}((\tau_k)_j^n)$, $(r_k)_j^n = (\rho_k)_j^n$ and

- $\overline{\alpha_k}_{j+1/2}(u_k)_{j+1/2}^{\star} = \overline{\alpha_k u_k}_{j+1/2} - \frac{\Delta(\alpha_k \pi_k)}{2a_k} + \frac{1}{2a_k}\{S_k\}_{j+1/2}^n$,
- $\overline{\alpha_k}_{j+1/2}(\alpha_k \pi_k)_{j+1/2}^{\star} = (\alpha_k)_j (\alpha_k)_{j+1}\left(\overline{\pi_k} - \frac{a_k}{2}\Delta u_k\right) + \frac{\Delta \alpha_k}{4}\{S_k\}_{j+1/2}^n$,
- $\{S_k\}_j^n = \frac{1}{2}\{S_k\}_{j+1/2}^n + \frac{1}{2}\{S_k\}_{j-1/2}^n$, with: $\{S_k\}_{j+1/2}^n = \overline{\pi_I}_{j+1/2} \Delta(\alpha_k)_{j+1/2}$,

where: $\overline{b}_{j+1/2} = \frac{b_{j+1} + b_j}{2}$, $\Delta b_{j+1/2} = b_{j+1} - b_j$.

4.2. **Treatment of the second step**

We now consider the numerical treatment of the time evolution corresponding to the second step. Starting from the output of the first step $\mathbb{U}_j^{\sharp}$, we want to compute the updated data at time t^{n+1}, $\mathbb{U}_j^{n+1}$. Denoting $\phi_k \in \{m_k, m_k u_k\}$, we use a standard time-explicit upwind discretization for the transport step by setting

$$\begin{array}{rcl}
(\phi_k)_j^{n+1} &=& (\phi_k)_j^{\sharp} - \frac{\Delta t}{\Delta x}\left((u_k)_{j+1/2}^{\star}(\phi_k)_{j+1/2}^{\sharp} - (u_k)_{j-1/2}^{\star}(\phi_k)_{j-1/2}^{\sharp}\right) \\
&& + \frac{\Delta t}{\Delta x}(\phi_k)_j^{\sharp}\left((u_k)_{j+1/2}^{\star} - (u_k)_{j-1/2}^{\star}\right), \\
(\alpha_1)_j^{n+1} &=& (\alpha_1)_j^{\sharp} - \frac{\Delta t}{\Delta x}\left((u_I)_{j+1/2}^{\star}(\alpha_1)_{j+1/2}^{\sharp} - (u_I)_{j-1/2}^{\star}(\alpha_1)_{j-1/2}^{\sharp}\right) \\
&& + \frac{\Delta t}{\Delta x}(\alpha_1)_j^{\sharp}\left((u_I)_{j+1/2}^{\star} - (u_I)_{j-1/2}^{\star}\right),
\end{array} \tag{28}$$

where

$$(\phi_k)^\sharp_{j+1/2} = \begin{cases} (\phi_k)^\sharp_j, & \text{if } (u_k)^\star_{j+1/2} \geq 0, \\ (\phi_k)^\sharp_{j+1}, & \text{if } (u_k)^\star_{j+1/2} < 0, \end{cases} \qquad (\alpha_1)^\sharp_{j+1/2} = \begin{cases} (\alpha_1)^\sharp_j, & \text{if } (u_I)^\star_{j+1/2} \geq 0, \\ (\alpha_1)^\sharp_{j+1}, & \text{if } (u_I)^\star_{j+1/2} < 0. \end{cases}$$

Let us note that the transport update (28) equivalently reads:

$$\begin{array}{rcl} (\phi_k)^{n+1}_j & = & (\phi_k)^\sharp_j L_j - \frac{\Delta t}{\Delta x}\left((u_k)^\star_{j+1/2}(\phi_k)^\sharp_{j+1/2} - (u_k)^\star_{j-1/2}(\phi_k)^\sharp_{j-1/2}\right), \\ (\alpha_1)^{n+1}_j & = & (\alpha_1)^\sharp_j L^I_j - \frac{\Delta t}{\Delta x}\left((u_I)^\star_{j+1/2}(\alpha_1)^\sharp_{j+1/2} - (u_I)^\star_{j-1/2}(\alpha_1)^\sharp_{j-1/2}\right), \\ L^I_j & = & 1 + \frac{\Delta t}{\Delta x}\left((u_I)^\star_{j+1/2} - (u_I)^\star_{j-1/2}\right). \end{array} \tag{29}$$

Let us note that the interface value of the velocity $(u_k)^\star_{j+1/2}$ coincides with the one proposed in the first step, which is actually crucial in order for the whole scheme to be conservative.

5. Two-step numerical method

In this section, we now give the details of the two-step process proposed in Section 3 for solving the barotropic Baer Nunziato model. Let us briefly recall that this two-step process is defined by

- Update $\mathbb{U}^n_j$ to $\mathbb{U}^\sharp_j$ by approximating the solution of (8).
- Update $\mathbb{U}^\sharp_j$ to $\mathbb{U}^{n+1}_j$ by approximating the solution of (9).

We begin with a fully explicit discretization of the Baer Nunziato model, which means that both steps of the process are solved with a time-explicit procedure, and we will go on with a mixed implicit-explicit strategy for which the solutions of (8) are solved implicitly in time and the solutions of (9) are solved explicitly. The latter strategy allows to get rid of the strong CFL restriction coming from the acoustic waves in the subsonic regime and corresponds to the motivation of the present study.

5.1. **Time-explicit discretization**

Let us begin with the time-explicit discretization of the acoustic system (8), or equivalently (10). The acoustic update is achieved thanks to the proposed relaxation approximation and the corresponding approximate Riemann solver detailed in Section 4.1. More precisely, we propose to simply use a Godunov-type method based on this approximate Riemann solver. If we focus on the conservative variable: $(\alpha_1, r_k, \alpha_k\rho_k, \alpha_k\rho_k u_k, r_k\pi_k)$, the discretization (27) yields the following formula for the acoustic update:

$$\left\{\begin{array}{rcl} (\alpha_1)^\sharp_j & = & (\alpha_1)^n_j, \\ (r_k)^\sharp_j & = & (r_k)^n_j, \\ L_j(\alpha_k\rho_k)^\sharp_j & = & (\alpha_k\rho_k)^n_j, \\ L_j(\alpha_k\rho_k u_k)^\sharp_j & = & (\alpha_k\rho_k u_k)^n_j - \frac{\Delta t}{\Delta x}\left((\alpha_k\pi_k)^\star_{j+1/2} - (\alpha_k\pi_k)^\star_{j-1/2}\right) + \Delta t\left\{\pi_I\partial_x\alpha_k\right\}^n_j, \\ (r_k\pi_k)^\sharp_j & = & (r_k\pi_k)^n_j - \frac{\Delta t}{\Delta x}a_k^2\left((u_k)^\star_{j+1/2} - (u_k)^\star_{j-1/2}\right), \\ L_j & = & 1 + \frac{\Delta t}{\Delta x}\left((u_k)^\star_{j+1/2} - (u_k)^\star_{j-1/2}\right). \end{array}\right. \tag{30}$$

Overall Discretization After injecting (30) in (29) one obtains the complete update procedure from t^n to t^{n+1} for the conservative variables:

$$\left\{\begin{array}{lcl}(\alpha_1)_j^{n+1} & = & (\alpha_1)_j^\sharp L_j^I - \frac{\Delta t}{\Delta x}\left((u_I)^\star_{j+1/2}(\alpha_1)^\sharp_{j+1/2} - (u_I)^\star_{j-1/2}(\alpha_1)^\sharp_{j-1/2}\right),\\ (\alpha_k\rho_k)_j^{n+1} & = & (\alpha_k\rho_k)_j^n - \frac{\Delta t}{\Delta x}\left((u_k)^\star_{j+1/2}(\alpha_k\rho_k)^\sharp_{j+1/2} - (u_k)^\star_{j-1/2}(\alpha_k\rho_k)^\sharp_{j-1/2}\right),\\ (\alpha_k\rho_k u_k)_j^{n+1} & = & (\alpha_k\rho_k u_k)_j^n - \frac{\Delta t}{\Delta x}\left((u_k)^\star_{j+1/2}(m_k u_k)^\sharp_{j+1/2} + (\alpha_k\pi_k)^\star_{j+1/2}\right.\\ & & \qquad\left. - (u_k)^\star_{j-1/2}(m_k u_k)^\sharp_{j-1/2} - (\alpha_k\pi_k)^\star_{j-1/2}\right) + \Delta t\left\{\pi_I\partial_x\alpha_k\right\}_j^n,\\ L_j^I & = & 1 + \frac{\Delta t}{\Delta x}\left((u_I)^\star_{j+1/2} - (u_I)^\star_{j-1/2}\right).\end{array}\right. \tag{31}$$

The next statement gathers the main properties satisfied by our explicit in time and two-step algorithm.

Proposition 5.1. *The fully explicit scheme (27)-(28) satisfies the following:*

(1) *The discretization of the partial masses $\alpha_k\rho_k$ is conservative*
(2) *The discretization of the total momentum $\alpha_1\rho_1u_1 + \alpha_2\rho_2u_2$ is conservative.*
(3) *The constant velocities/pressures profiles are preserved.*
(4) *Under the Whitham subcharacteristic condition* (13) *and the CFL conditions*

$$\frac{\Delta t}{\Delta x}\max_{j\in\mathbb{Z}}\max_{k\in\{1,2\}}|\,(a_k\tau_k)_j^n\,| < \frac{1}{2}, \qquad \frac{\Delta t}{\Delta x}\max_{j\in\mathbb{Z}}\left(((u_k)^\star_{j-1/2})^+ - ((u_k)^\star_{j+1/2})^-\right) < 1, \tag{32}$$

the scheme preserves the maximum principle for the phase fractions: $0 < \alpha_k < 1$ and positive values of the densities $\rho_k > 0$.

Proof.

(1) This is a straightforward consequence of (31).
(2) Summing the momentum equations in system (31) over k yields:

$$\begin{array}{lcl}(\alpha_1\rho_1u_1 + \alpha_2\rho_2u_2)_j^{n+1} & = & (\alpha_1\rho_1u_1 + \alpha_2\rho_2u_2)_j^n - \frac{\Delta t}{\Delta x}\left((\alpha_1\pi_1 + \alpha_2\pi_2)^{\star L}_{j+1/2} - (\alpha_1\pi_1 + \alpha_2\pi_2)^{\star R}_{j-1/2}\right.\\ & & \quad + (u_1)^\star_{j+1/2}(\alpha_1\rho_1u_1)^\sharp_{j+1/2} - (u_1)^\star_{j-1/2}(\alpha_1\rho_1u_1)^\sharp_{j-1/2}\\ & & \quad\left. + (u_2)^\star_{j+1/2}(\alpha_2\rho_2u_2)^\sharp_{j+1/2} - (u_2)^\star_{j-1/2}(\alpha_2\rho_2u_2)^\sharp_{j-1/2}\right).\end{array}$$

As $\alpha_1\pi_1 + \alpha_2\pi_2$ is a Riemann invariant of the standing wave for the relaxation acoustic system (12), we have $(\alpha_1\pi_1 + \alpha_2\pi_2)^{\star L}_{j+1/2} = (\alpha_1\pi_1 + \alpha_2\pi_2)^{\star R}_{j+1/2}$, which preserves the conservative form.

(3) Let us consider the state:

$$\left((\alpha_1)_j^n, (\alpha_k\rho_k)_j^n, (\alpha_k\rho_k u_k)_j^n\right) = \left((\alpha_1)_j^n, (\alpha_k)_j^n\rho_k(\overline{p}), (\alpha_k)_j^n\rho_k(\overline{p})\overline{u}\right), \quad (\alpha_k)_j^n \in (0,1), \quad k = 1,2,$$

with constant velocities $\overline{u}$ and pressures $\overline{p}$. Injecting this state in the two-step numerical method (31), we obtain:

$$\left((\alpha_1)_j^{n+1}, (\alpha_k\rho_k)_j^{n+1}, (\alpha_k\rho_k u_k)_j^{n+1}\right) = \left((\alpha_1)_j^{n+1}, (\alpha_k)_j^{n+1}\rho_k(\overline{p}), (\alpha_k)_j^{n+1}\rho_k(\overline{p})\overline{u}\right), \quad (\alpha_k)_j^{n+1} \in (0,1), \quad k = 1,2.$$

(4) Thanks to (30), the CFL condition (32) ensures that $(\rho_k)_j^\sharp > 0$ and $0 < (\alpha_k)_j^\sharp < 1$ for $j \in \mathbb{Z}$. The CFL condition (32) yields that $(\rho_k)_j^{n+1}$ and $(\alpha_k)_j^{n+1}$ are convex combinations of $(\rho_k)_l^\sharp$ and $(\alpha_k)_l^\sharp$ respectively for $l = j \pm 1, j$ and therefore $(\rho_k)_j^{n+1} > 0$ and $0 < (\alpha_k)_j^{n+1} < 1$.

□

5.2. **Semi-implicit discretization**

Let us now consider the last algorithm of this paper. It consists in considering a time-implicit scheme for the acoustic step and keeping unchanged the transport step. This strategy will allow us to obtain a stable algorithm under a CFL restriction based on the material velocity u_k and not on the sound velocity c_k. In order to derive a time-implicit scheme for the acoustic step, we follow the following standard approach where the numerical fluxes are now evaluated at time $t^\sharp$, that gives here the same update formulas as in the explicit case but where the numerical fluxes now involve quantities at time $t^\sharp$ apart from the term consistent with $\{\pi_I \partial_x \alpha_k\}$, which writes:

- $\overline{\alpha_k}_{j+1/2}((u_k)^\star_{j+1/2})^\sharp = \overline{\alpha_k u_k}^\sharp_{j+1/2} - \frac{\Delta(\alpha_k\pi_k)^\sharp}{2a_k} + \frac{1}{2a_k}\{S_k\}^n_{j+1/2}$,
- $\overline{\alpha_k}_{j+1/2}((\alpha_k\pi_k)^\star_{j+1/2})^\sharp = (\alpha_k)_j(\alpha_k)_{j+1}\left(\overline{\pi_k}^\sharp - \frac{a_k}{2}\Delta u_k^\sharp\right) + \frac{\Delta\alpha_k}{4}\{S_k\}^n_{j+1/2}$.

Let us observe that we suggest here to keep on evaluating the interfacial pressure source term at time t^n. It is interesting to see that it is equivalent to the following system written in characteristic variables:

$$
\begin{aligned}
(\alpha_1)^\sharp_j &= (\alpha_1)^n_j,\\
(r_k)^\sharp_j &= (r_k)^n_j,\\
(\tau_k)^\sharp_j &= (\tau_k)^n_j + \frac{\lambda}{(r_k)^n_j}\left((u_k^\star)^\sharp_{j+1/2} - (u_k^\star)^\sharp_{j-1/2}\right),\\
(\overrightarrow{W}_k)^\sharp_j &= (\overrightarrow{W}_k)^n_j - \frac{\lambda a_k}{(r_k)^n_j}(\overrightarrow{W}_k)^\sharp_j + \frac{\lambda a_k(\alpha_k)^n_{j-1}}{(r_k)^n_j(\overline{\alpha_k})_{j-1/2}}(\overrightarrow{W}_k)^\sharp_{j-1} - \frac{\lambda a_k(\Delta\alpha_k)_{j-1/2}}{2(r_k)^n_j(\overline{\alpha_k})_{j-1/2}}(\overleftarrow{W}_k)^\sharp_j\\
&\qquad + \frac{\lambda a_k}{(\overline{\alpha_k})_{j-1/2}(r_k)^n_j}\{S\}^n_{j-1/2},\\
(\overleftarrow{W}_k)^\sharp_j &= (\overleftarrow{W}_k)^n_j - \frac{\lambda a_k}{(r_k)^n_j}(\overleftarrow{W}_k)^\sharp_j + \frac{\lambda a_k(\alpha_k)^n_{j+1}}{(r_k)^n_j(\overline{\alpha_k})_{j+1/2}}(\overleftarrow{W}_k)^\sharp_{j+1} + \frac{\lambda a_k(\Delta\alpha_k)_{j+1/2}}{2(r_k)^n_j(\overline{\alpha_k})_{j+1/2}}(\overrightarrow{W}_k)^\sharp_j\\
&\qquad - \frac{\lambda a_k}{(\overline{\alpha_k})_{j+1/2}(r_k)^n_j}\{S\}^n_{j+1/2},
\end{aligned}
\tag{33}
$$

where the new variables $\overleftarrow{W}_k$ and $\overrightarrow{W}_k$ are defined by $\overrightarrow{W}_k = \pi_k + a_k u_k$, $\overleftarrow{W}_k = \pi_k - a_k u_k$. These quantities are the Riemann invariants associated with the characteristic speeds $\pm a_k\tau_k$ of the relaxation system (14). We firstly compute $\overleftarrow{W}_k$ and $\overrightarrow{W}_k$. Once this is done, τ_k variables can be updated explicitly since $((u_k)^\star_{j\pm1/2})^\sharp$ is explicitly known from the knowledge of $\overleftarrow{W}_k^{\ \sharp}$ and $\overrightarrow{W}_k^{\ \sharp}$ by the formulas

$$
(u_k)^\sharp_j = \frac{1}{2a_k}\left((\overrightarrow{W}_k)^\sharp_j - (\overleftarrow{W}_k)^\sharp_j\right), \qquad (\pi_k)^\sharp_j = \frac{1}{2}\left((\overrightarrow{W}_k)^\sharp_j + (\overleftarrow{W}_k)^\sharp_j\right).
$$

Remark 5.2. In the semi-implicit Lagrange projection, we need to solve a linear system to update the solution at time $t^\sharp$.

$$
\begin{pmatrix} A_{\overrightarrow{W}_k,\overrightarrow{W}_k} & A_{\overrightarrow{W}_k,\overleftarrow{W}_k} \\ A_{\overleftarrow{W}_k,\overrightarrow{W}_k} & A_{\overleftarrow{W}_k,\overleftarrow{W}_k} \end{pmatrix}
\begin{pmatrix} \overrightarrow{W}_k \\ \overleftarrow{W}_k \end{pmatrix} =
\begin{pmatrix} B_{\overrightarrow{W}_k} \\ B_{\overleftarrow{W}_k} \end{pmatrix},
\tag{34}
$$

where the block matrices $A_{\overrightarrow{W}_k,\overrightarrow{W}_k}$ and $A_{\overleftarrow{W}_k,\overleftarrow{W}_k}$ are bidiagonal and the block matrices $A_{\overrightarrow{W}_k,\overleftarrow{W}_k}$ and $A_{\overleftarrow{W}_k,\overrightarrow{W}_k}$ are diagonal. The implementation of this sparse matrix is made by the use of the Python library "*scipy.sparse*" and we solve the linear system (34) with a direct method from "*scipy.sparse.spsolve*".

Proposition 5.3. *The implicit-explicit scheme (33)-(28) satisfies the following:*

- *The discretization of the partial masses $\alpha_k\rho_k$ is conservative*
- *The discretization of the total momentum $\alpha_1\rho_1u_1 + \alpha_2\rho_2u_2$ is conservative.*

- *The constant velocities/pressures profiles are preserved.*

Under the Whitham subcharacteristic condition and the CFL conditions,

$$\frac{\Delta t}{\Delta x}\max_{j\in\mathbb{Z}}\left(((u_k)^\star_{j-1/2})^+ - ((u_k)^\star_{j+1/2})^-\right) < 1 \tag{35}$$

- *It preserves the maximum principle for the phase fractions:* $0 < \alpha_k < 1$ *and positive values of the densities* $\rho_k > 0$.

Proof. The properties are obtained in the same way as in the explicit case. □

6. Numerical results

In this section, we present three test cases that are representative of the numerical challenges of the BN model: the vanishing phase and the capture of a pure contact discontinuity. Here, we compare the approximate solution computed with our two-step numerical scheme, with a reference solution. For the first and the second test cases, the reference solution is computed over a 10^5 cells mesh with the Rusanov scheme. In the last test case, the reference solution is the exact solution of the Riemann problem.

These three test cases are Riemann problems defined from the variables $\mathbb{V} := (\alpha_1, \rho_1, u_1, \rho_2, u_2)$ by setting the initial data as:

$$\mathbb{V}(t=0,x) = \begin{cases} \mathbb{V}_L \text{ if } x < 0.5, \\ \mathbb{V}_R \text{ if } x > 0.5. \end{cases}$$

In these cases, the phasic equations of state are given by the following ideal gas pressure laws:

$$\begin{array}{l} p_1(\rho_1) = \kappa_1\rho_1^{\gamma_1}, \text{ with } \kappa_1 = 1 \text{ and } \gamma_1 = 2, \\ p_2(\rho_2) = \kappa_2\rho_2^{\gamma_2}, \text{ with } \kappa_2 = 1 \text{ and } \gamma_2 = 3. \end{array} \tag{36}$$

The solutions are computed on the domain $[0,1]$ of the x-space. For all the test cases, a mesh refinement process is implemented in order to numerically check the convergence of the method. For this purpose, we compute the discrete L^1 error between the approximate solution and a reference solution at the final time T, normalized by the discrete L^1 norm of the reference solution for both tests 1 and 2. For the last test case, the reference solution is the exact one.

$$\text{error}(\Delta x) = \frac{\sum_j |\mathbb{V}_j^n - \mathbb{V}_{\text{ref}}(x_j,T)|}{\sum_j |\mathbb{V}_{\text{ref}}(x_j,T)|}, \tag{37}$$

The calculations have been implemented on several uniform meshes. The coarser mesh is composed of 100 cells and the more refined one contains 5×10^4 cells. The error (37) is then plotted against Δx in a $\log-\log$ scale in Figures 3, 6, 9.

6.1. **Test case 1: a complete Riemann problem**

We consider a first test that displays all the waves: acoustic waves and contact discontinuity, with the following initial data [16],

$$\begin{array}{rcl} \mathbb{V}_L & = & (0.1,\ 0.85,\ 0.4609513139,\ 0.96,\ 0.0839315299) \text{ if } x < 0.5, \\ \mathbb{V}_R & = & (0.6,\ 1.2520240113,\ 0.7170741165,\ 0.2505659851,\ -0.3764790609) \text{ if } x > 0.5. \end{array}$$

The exact solution is composed of a $(u_1 - c_1)$-shock wave, followed by a $(u_2 - c_2)$-rarefaction wave, followed by a u_2-contact discontinuity, followed by a $(u_2 + c_2)$-shock and finally followed by a $(u_1 + c_1)$-rarefaction wave.

In Figures 1, 2, the approximate solution computed with the explicit and implicit-explicit Lagrange projection schemes are compared with both a reference solution computed over a 10^5 cells mesh with the Rusanov scheme and the approximate solution obtained with Rusanov scheme. We first observe that the implicit scheme is the most diffusive, which was clearly expected from the implicit treatment of the acoustic step. Note also

that our Lagrange-Projection schemes correctly capture the intermediate states even for this rather coarse mesh of 1000 cells. It appears that the contact discontinuity is captured more sharply by the explicit Lagrange projection method than by Rusanov scheme for which the numerical diffusion is larger. The two Lagrange projection schemes are comparable to the results given by the relaxation scheme introduced in [15] (see page 34). Nevertheless, we observe that the ImEx method generates an overshoot at the contact discontinuity where the phase fraction α_k jumps. This oscillation is reduced on a finer mesh of 10000 cells in Figure 2 and does not generate an instability. To have a better understanding of this behavior at the contact discontinuity, we study a Riemann problem with a stationnary contact discontinuity in the last test case. The appearance of all the waves in this first test case and of their numerical diffusion can make the interpretation of the results difficult. Figure 3 also shows that the approximate solution computed thanks to the Lagrange Projection schemes converges towards the reference solution. The errors converge towards zero with a rate between $\Delta x^{1/2}$ and Δx. The expected order of $\Delta x^{1/2}$ could be otained by implementing the calculation on much more refined meshes in order to recover this asymptotic order of convergence.
Table 1 gives for each test case the number of iterations needed to perform the computations. As expected, the gain is important when using the proposed implicit-explicit algorithm and the corresponding CFL restriction based on the material waves (instead of the acoustic waves as for the explicit scheme).

	Test 1	Test 2	Test 3
Rusanov	808	780	688
LP explicit	616	729	672
LP implicit	203	214	398

TABLE 1. Number of time-iterations for each test case with 1000 cells

6.2. **Test case 2: vanishing phase**

We now consider a Riemann problem in which one of the two phases vanishes in one of the initial states. That means that the corresponding phase fraction α_1 or α_2 is equal to zero. This configuration poses a difficulty in the two-fluid model owing to its independent velocities. The singularity arises when one computes the absent phase velocity using the conservative variables $u_k = \frac{\alpha_k \rho_k u_k}{\alpha_k \rho_k}$.
For this kind of Riemann problem, the u_I-contact separates a mixture region where the two phases coexist from a single phase region with the remaining phase. Assuming for instance that $\alpha_1^L = 1$ and $0 < \alpha_1^R < 1$, the right state is a mixture of both phases while the left initial state is composed solely of phase 1. We consider the following initial data [16],

$$\begin{aligned} \mathbb{V}_L &= (1,\ 1.8,\ 0.747051068928543,\ 3.979765198025580,\ 0.6) \quad \text{if } x < 0.5, \\ \mathbb{V}_R &= (0.4,\ 2.081142099494683,\ 0.267119045902047,\ 5.173694757433254,\ 1.069067604724276) \quad \text{if } x > 0.5. \end{aligned}$$

The exact solution is composed of a $(u_1 - c_1)$-shock wave in the left-hand side region where only phase 1 is present. This region is separated by a u_I-contact discontinuity from the right-hand side region where the two phases are mixed. In this RHS region, the solution is composed of a $(u_2 + c_2)$-rarefaction wave followed by a $(u_1 + c_1)$-rarefaction wave. In practice, the numerical method requires values of α_1^L and α_1^R that lie strictly in the interval $(0, 1)$. Therefore, in the numerical implementation, we take $\alpha_1^L = 1 - 10^{-9}$. The aim here is to give a qualitative comparison between the numerical approximation and the reference solution. Moreover, there is theoretically no need to specify left initial values for the phase 2 quantities since this phase is not present in the LHS region. For the sake of the numerical simulations however, one must provide such values. We choose to set ρ_2^L and u_2^L to the values on the right of the u_I-contact discontinuity. As for the first test case, we can see in Figures 4,5 that for the same level of refinement, the explicit Lagrange projection scheme is more accurate than Rusanov scheme. That can be seen especially for phase 1. As regards the region where phase 2 does not exist, we can see that the three numerical schemes develop some oscillations when it comes to divisions by

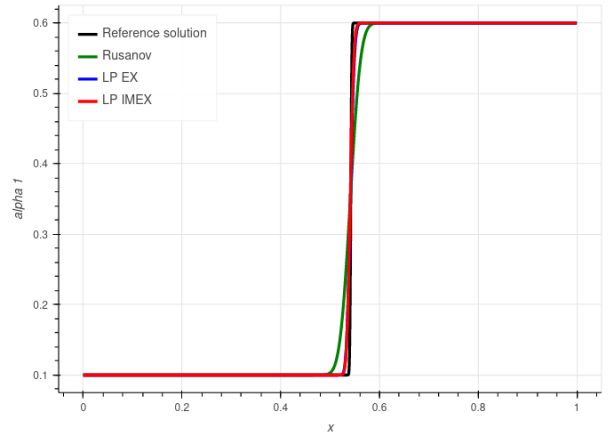

(A) Phase 1 fraction α_1

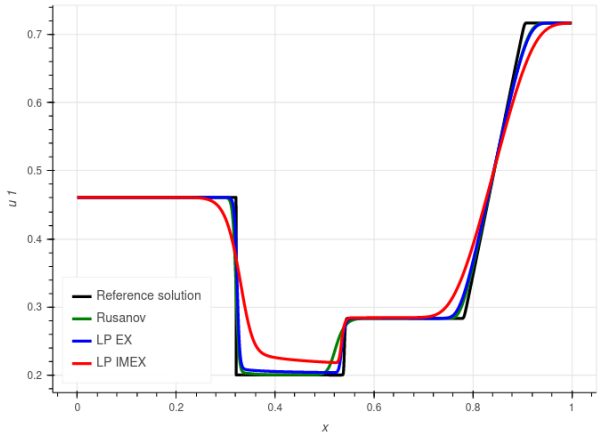

(B) Phase 1 velocity u_1

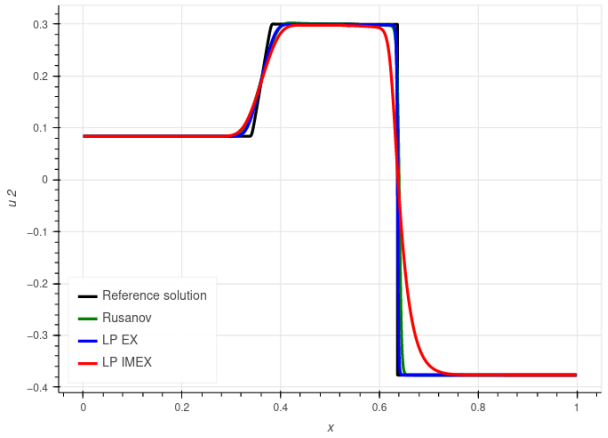

(C) Phase 2 velocity u_2

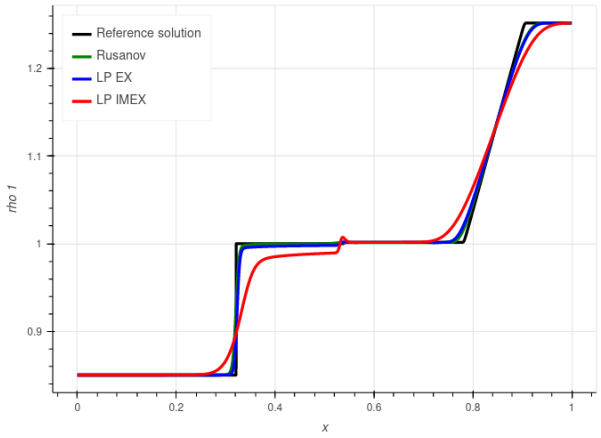

(D) Phase 1 density ρ_1

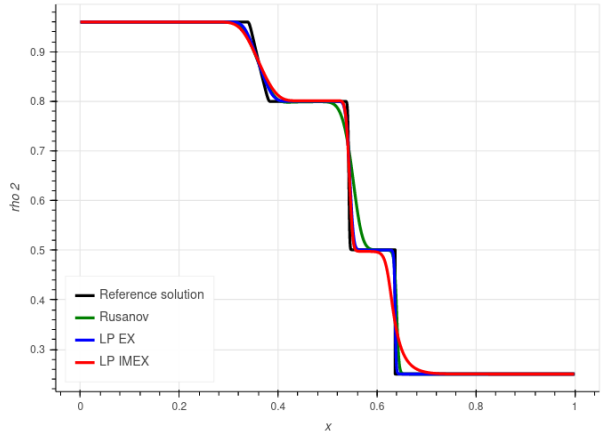

(E) Phase 2 density ρ_2

FIGURE 1. Test case 1: Space variations of the physical variables at the final time $T = 0.14$. Mesh size: 1000 cells.

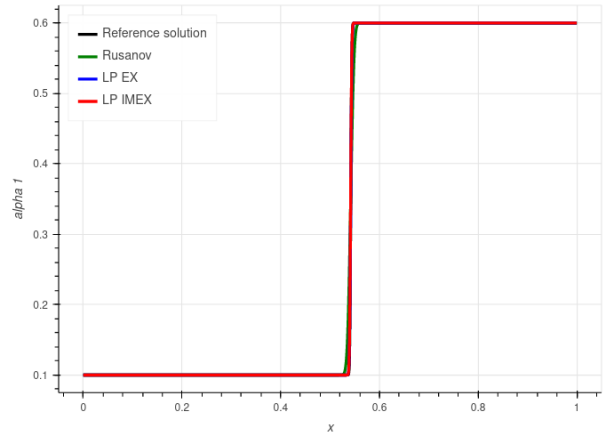

(A) Phase 1 fraction α_1

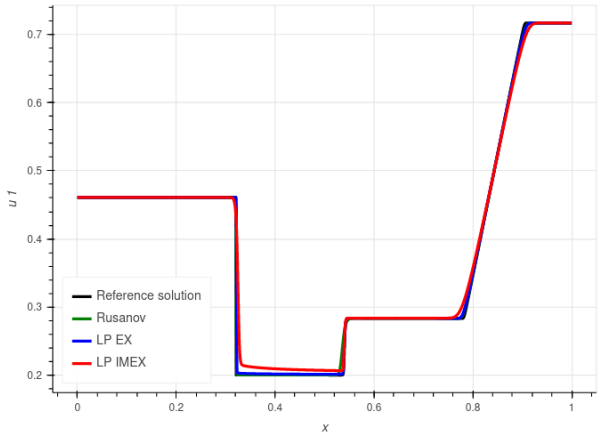

(B) Phase 1 velocity u_1

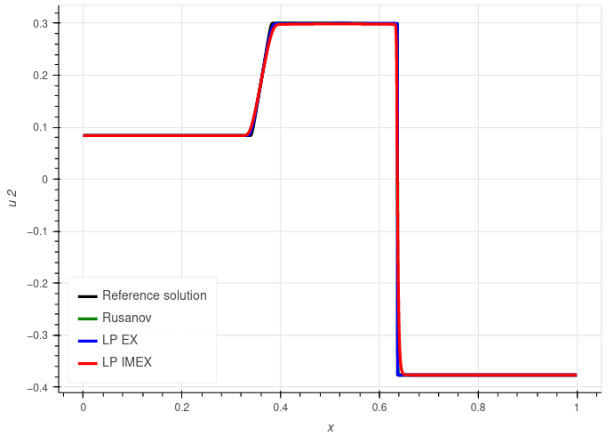

(C) Phase 2 velocity u_2

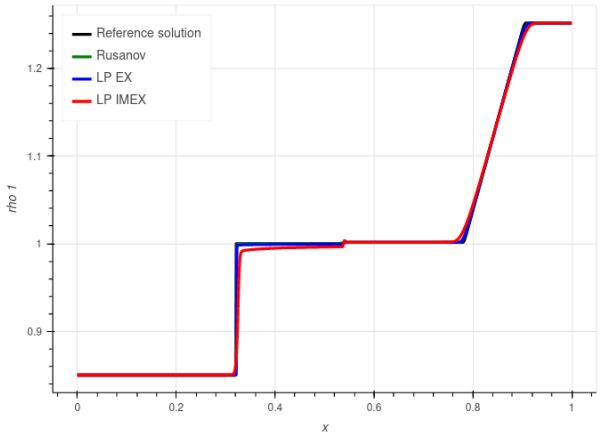

(D) Phase 1 density ρ_1

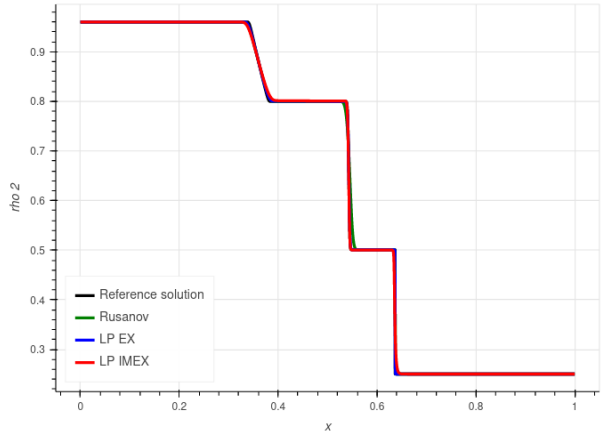

(E) Phase 2 density ρ_2

FIGURE 2. Test case 1: Space variations of the physical variables at the final time $T = 0.14$. Mesh size: 10000 cells.

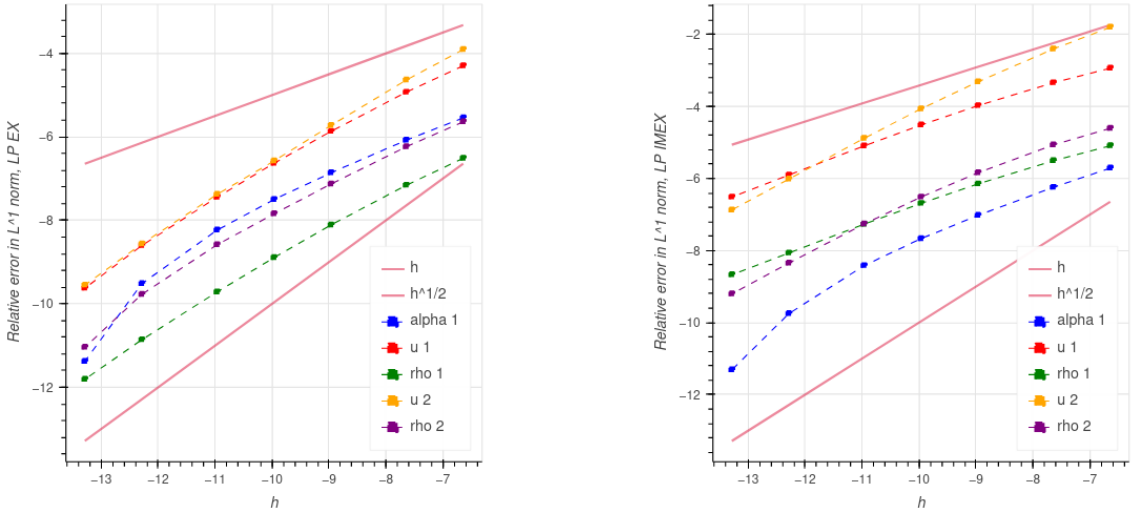

(A) Explicit Lagrange Projection scheme (B) IMEX Lagrange Projection scheme

FIGURE 3. Test case 1: Convergence study. Mesh size: 100 to 10^4 cells.

small values of α_2. This behavior is also observed with the relaxation scheme in [15] (see page 37). The ImEx method also generates an oscillation at the location where the phase fraction α_2 jumps and is more diffusive for the capture of the $(u_1 + c_1)$-rarefaction wave (see Phase 1 density in Figure 4). The oscillation and numerical diffusion are lower on a finer mesh of 10000 cells in Figure 2 and ImEx method converges towards the reference solution.

Figure 6 also shows that the approximate solution computed thanks to the Lagrange Projection schemes converge towards the reference solution. The errors converge towards zero with a rate between $\Delta x^{1/2}$ and Δx. The expected order of $\Delta x^{1/2}$ could be otained by implementing the calculation on much more refined meshes in order to recover this asymptotic order of convergence.

6.3. **Test case 3: a pure contact discontinuity**

In the last test case, we seek to analyze the behavior of the explicit and ImEx Lagrange Projection (LP) schemes and the Rusanov scheme for the capture of a pure stationnary contact discontinuity. This Riemann problem is built following the procedure explained in Appendix B. Here, in the exact solution, all the physical quantities are transported with the constant velocity $u_I = 0$. The initial data is defined as

$$\begin{array}{rcll} \mathbb{V}_L & = & (0.8,\ 7.0710678118654755,\ 0.4448746176198241,\ 3.7907146169832258,\ 0) & \text{if } x < 0.5, \\ \mathbb{V}_R & = & (0.2,\ 3.1622776601683795,\ 3.979079545848609,\ 3.6840314986403864,\ 0) & \text{if } x > 0.5. \end{array} \tag{38}$$

Figures 7 and 8 gather the curves of $(\alpha_1, \rho_1, u_1, \rho_2, u_2)$ as functions of x and Figure 9 gathers the L^1 relative error compared to the initial state for the variables $(\alpha_1, \rho_1, u_1, \rho_2)$, and the L^1 absolute error for u_2 (as $|u_2| = 0$ everywhere).

The approximation of a pure contact discontinuity represents a challenging test case. Indeed, for all schemes considered in the present article, including the Rusanov scheme several pathological phenomena can be observed.

First, none of the numerical schemes succeeded in perfectly preserving the zero-velocity $u_I = u_2$ profile. Such an error on u_2 also induces an error on ρ_2 as it its profile cannot be kept stationary. Nevertheless, u_2 seems to converge to zero (in L^1) with both Acoustic-Transport schemes, but not with the Rusanov scheme.

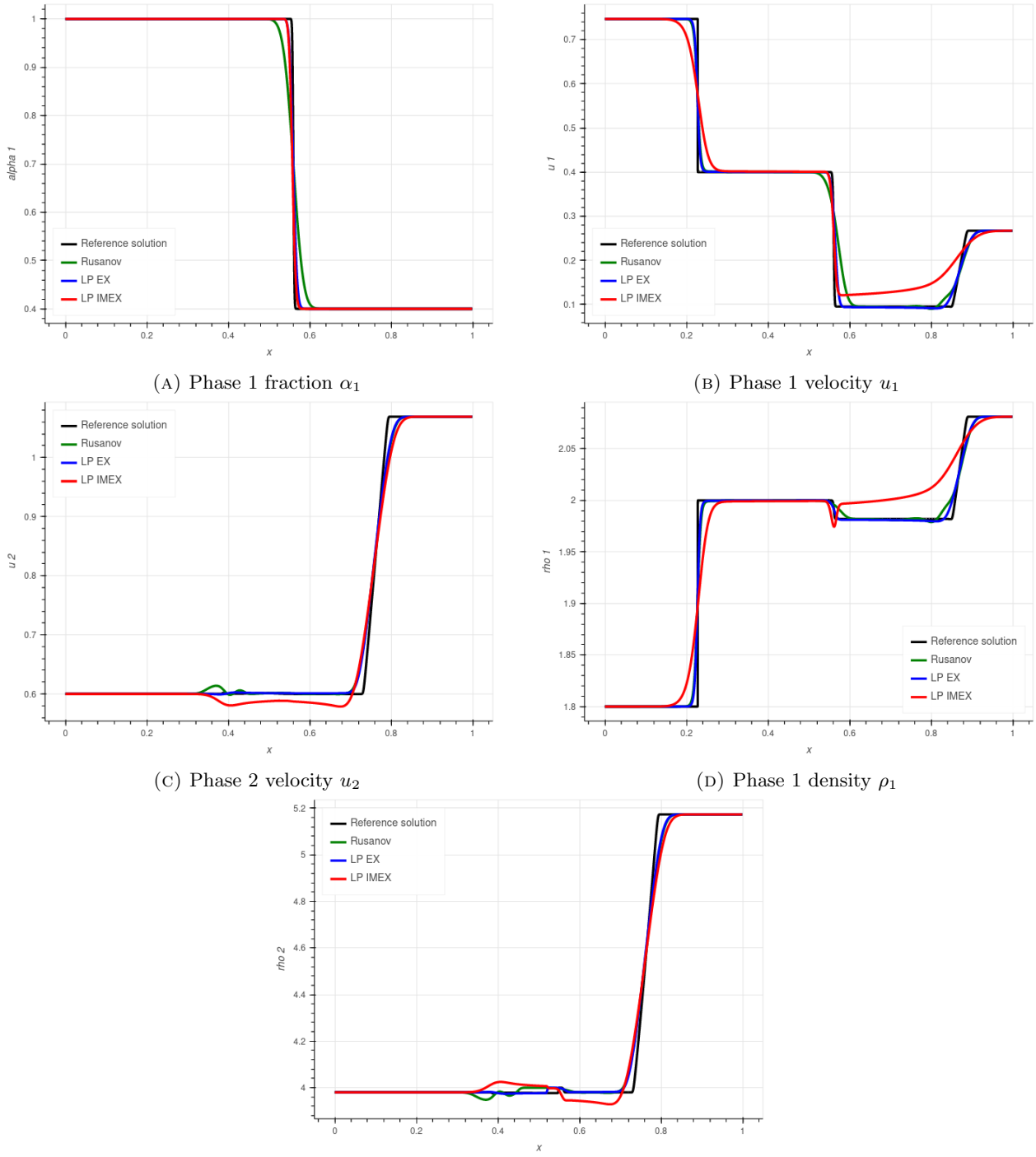

(A) Phase 1 fraction α_1

(B) Phase 1 velocity u_1

(C) Phase 2 velocity u_2

(D) Phase 1 density ρ_1

(E) Phase 2 density ρ_2

FIGURE 4. Test case 2: Space variations of the physical variables at the final time $T = 0.1$. Mesh size: 1000 cells.

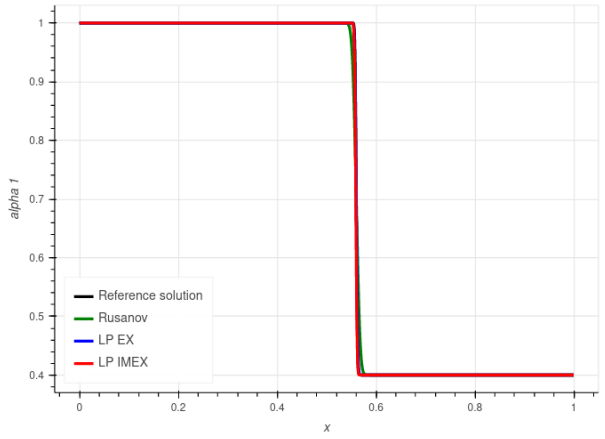

(A) Phase 1 fraction α_1

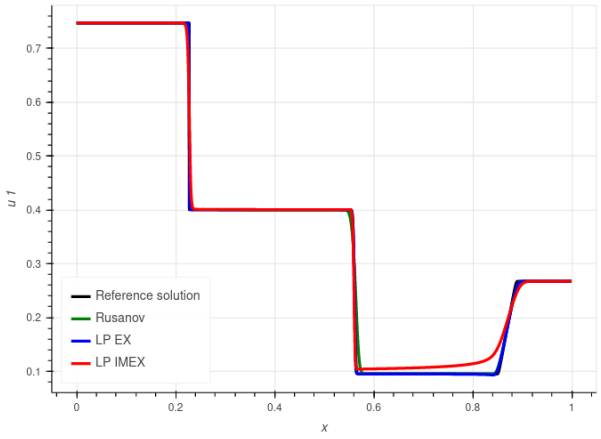

(B) Phase 1 velocity u_1

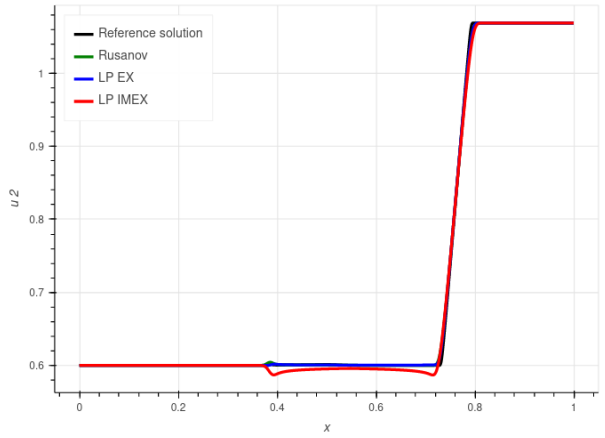

(C) Phase 2 velocity u_2

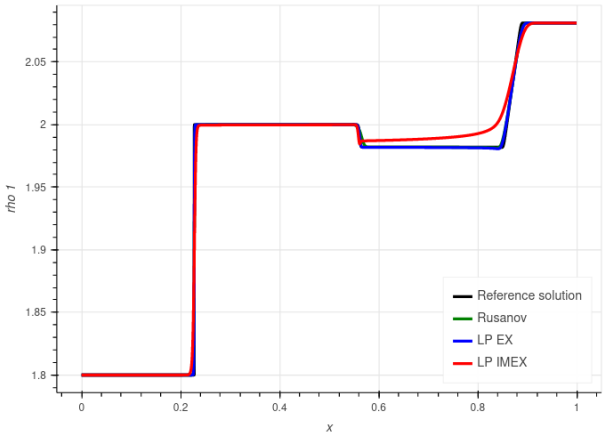

(D) Phase 1 density ρ_1

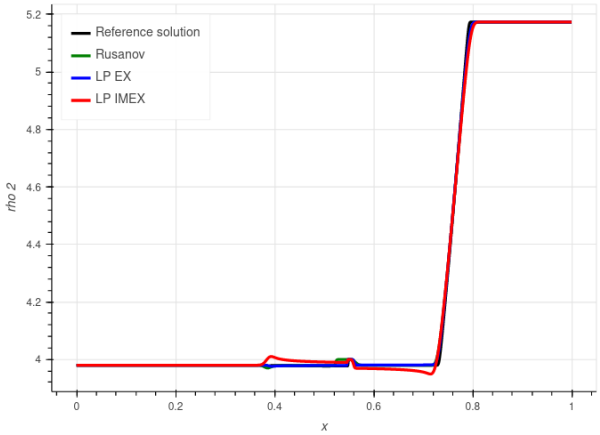

(E) Phase 2 density ρ_2

FIGURE 5. Test case 2: Space variations of the physical variables at the final time $T = 0.1$. Mesh size: 10000 cells.

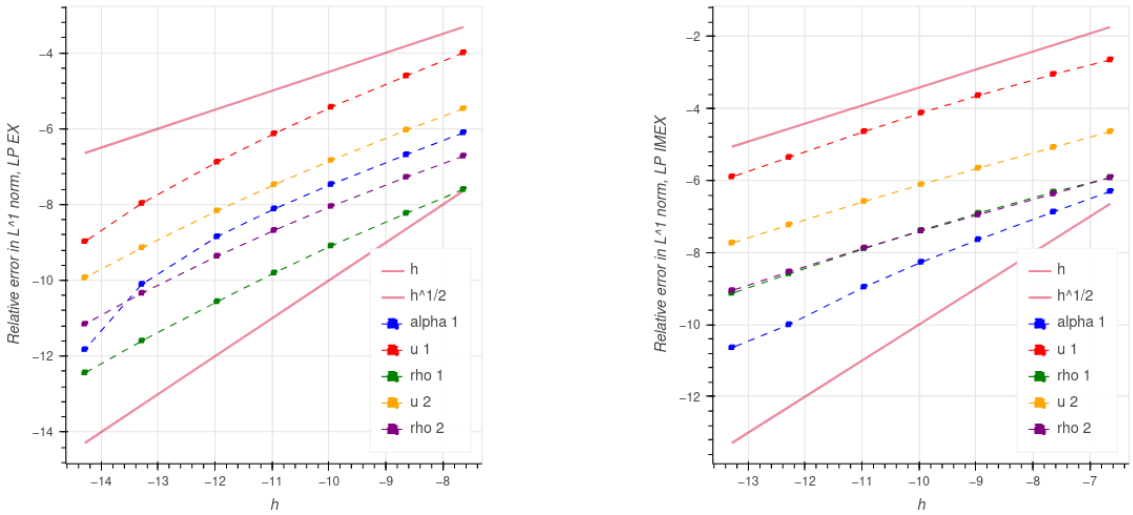

(A) Explicit Lagrange Projection scheme (B) IMEX Lagrange Projection scheme

FIGURE 6. Test case 2: Convergence study. Mesh size: 100 to 10^4 cells.

For the ρ_1 profile, both Acoustic-Transport schemes produce an overshoot at the location of the discontinuity. This results from the computation $\rho_1 = (\alpha_1\rho_1)/\alpha_1$. This overshoot reduces when using a finer mesh. It is not observed with the Rusanov scheme that is more diffusive. Moreover, on the right-side of the contact discontinuity, ρ_1 seems to evolve as a regular solution over an important part of the computational domain and then finally reaches a plateau value on the right side of the domain. Even for finer meshes, the solution does not seem to converge towards the initial state when $\Delta x \to 0$. The same problem appears on the u_1 profile. Moreover, this very pathological behavior was also obtained with the relaxation scheme [15] (the simulations with the relaxation scheme [15] were performed by K. Saleh). Let us mention that the problem of capturing correct profiles for the coupling wave in BN models has been successfully investigated by [1] by the mean of an approximate Riemann solver.

7. CONCLUSIONS

We proposed in this work an extension of the Lagrange-Projection decomposition for the barotropic BN model by means of an operator splitting strategy. We studied both a full explicit time discretization and an implicit-explicit method that enables the use of time steps constrained by CFL conditions that do not involve the sound velocity of the fluids. Both the full-explicit and implicit-explicit methods are shown to ensure maximum principle for the volume fractions α_k and positive values of the densities ρ_k. Future work include entropy analysis through the Lagrange projection splitting, extension of the strategy to multi-dimensional problems and to the full Baer-Nunziato model with energy equations.

This work was supported by a grant from Région Ile-de-France DIM MATHINNOV and the project AID Écoles (École polytechnique, ENSTA, ONERA, CentraleSupélec) MMEED (Reduced-order multi-scale modeling of two-phase flows with strong couplings between phases: from primary atomization to turbulent dispersed-phase flows - PI. M. Massot and T. Pichard at École polytechnique and R. Monchaux at ENSTA) 2020-2024.
The authors would like to thank K. Saleh for his advices and his help in performing the numerical simulation of the pure contact discontinuity test case with the relaxation scheme.

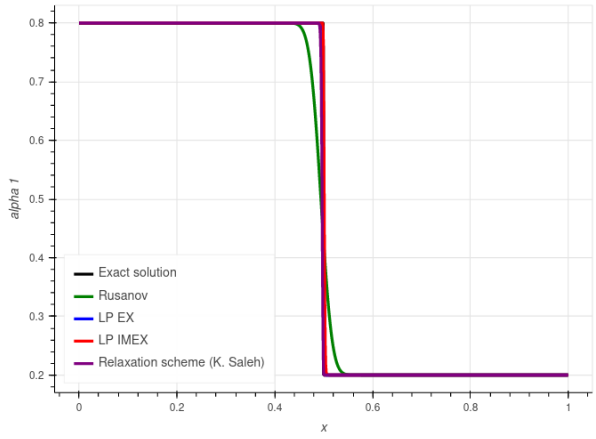

(A) Phase 1 fraction α_1

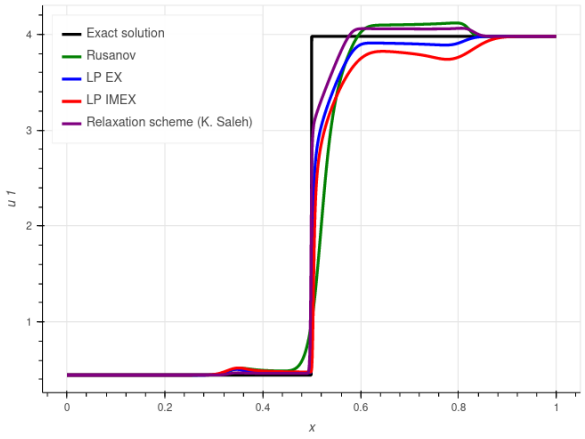

(B) Phase 1 velocity u_1

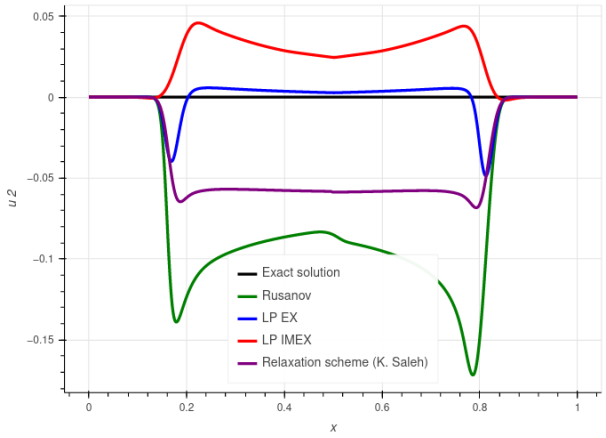

(C) Phase 2 velocity u_2

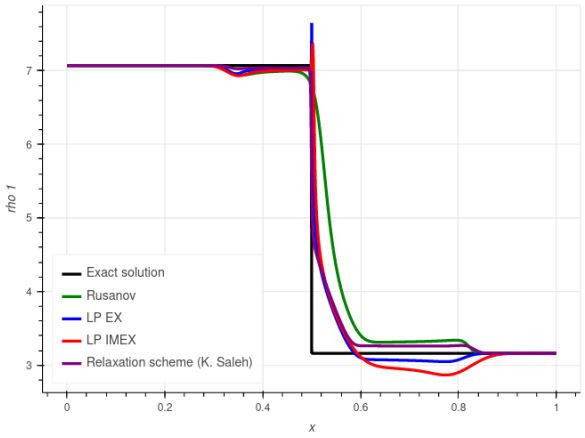

(D) Phase 1 density ρ_1

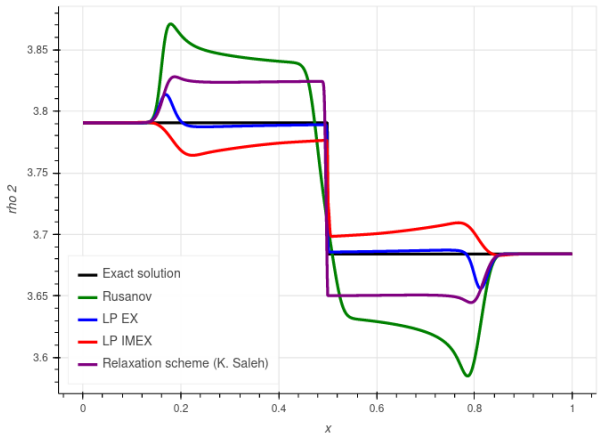

(E) Phase 2 density ρ_2

FIGURE 7. Test case 3: Structure of the solution and space variations of the physical variables at the final time $T = 0.05$. Mesh size: 1000 cells.

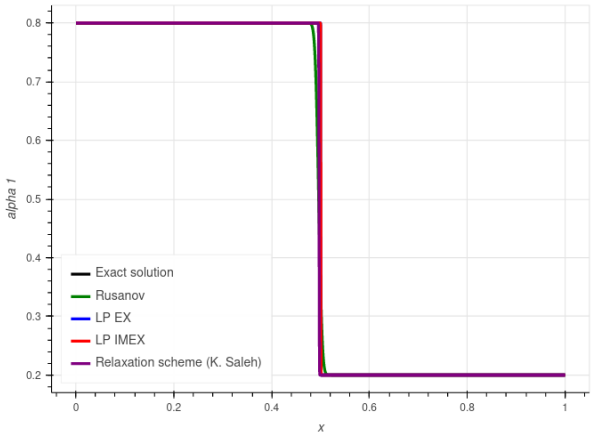

(A) Phase 1 fraction α_1

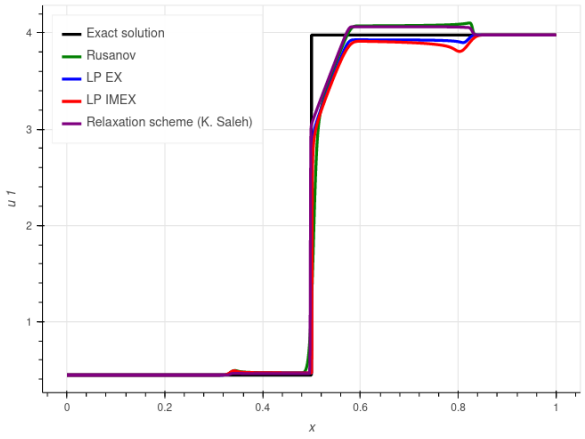

(B) Phase 1 velocity u_1

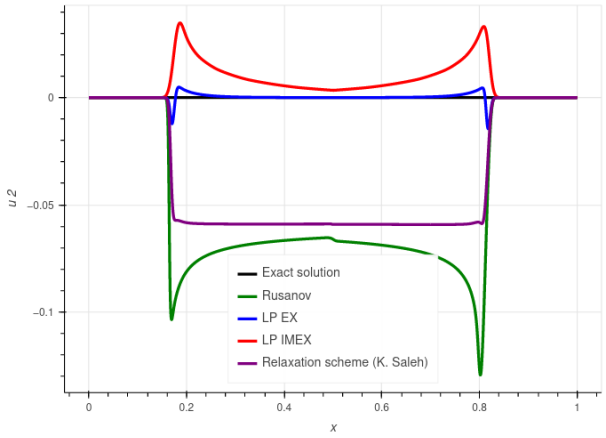

(C) Phase 2 velocity u_2

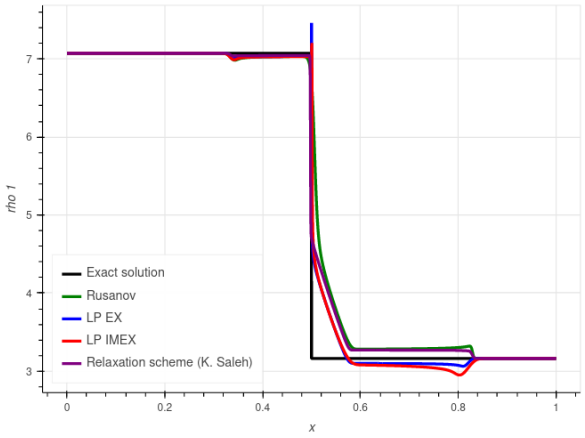

(D) Phase 1 density ρ_1

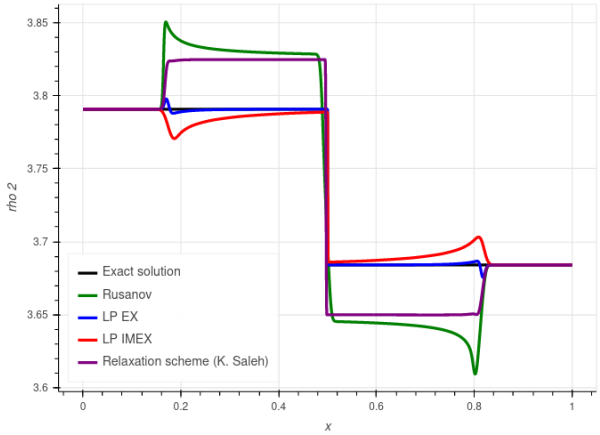

(E) Phase 2 density ρ_2

FIGURE 8. Test case 3: Structure of the solution and space variations of the physical variables at the final time $T = 0.05$. Mesh size: 10000 cells.

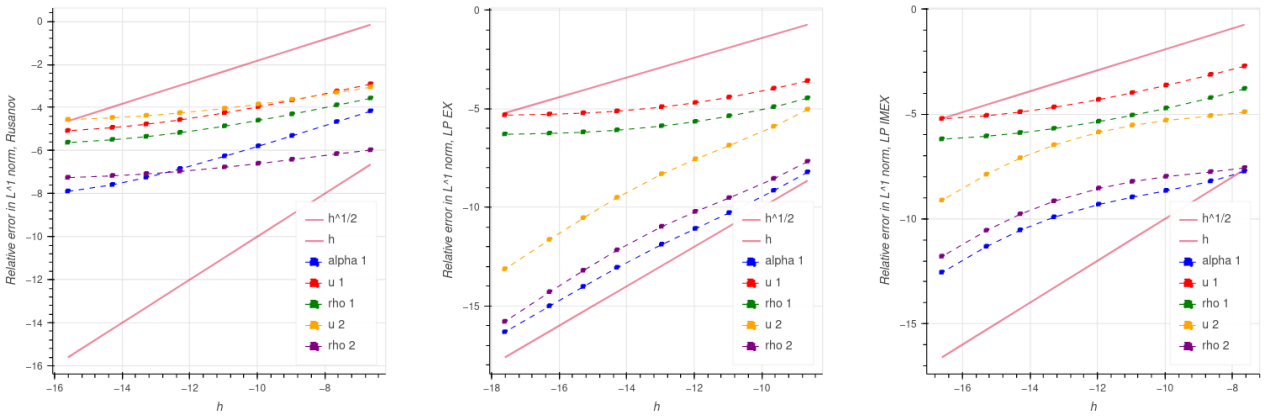

(A) Rusanov (B) Explicit Lagrange Projection (C) IMEX Lagrange Projection

FIGURE 9. Test case 3: Convergence study. Mesh size: 100 to 5×10^4 cells.

A. EIGENSTRUCTURE OF THE RELAXED ACOUSTIC SYSTEM

Considering smooth solutions, the relaxed acoustic system (14) reads

$$\partial_t W + A(W)\partial_x W = 0, \quad A = \begin{pmatrix} 0 & 0 & 0 & 0 & 0 & 0 & 0 & 0 & 0 \\ 0 & 0 & 0 & 0 & 0 & 0 & 0 & 0 & 0 \\ \frac{u_1}{\alpha_1} & \frac{u_1}{r_1} & 0 & -\frac{1}{r_1\alpha_1} & 0 & 0 & 0 & 0 & 0 \\ \pi_1 - \pi_I & -\frac{\alpha_1\pi_1}{r_1} & 0 & 0 & \frac{\alpha_1}{r_1} & 0 & 0 & 0 & 0 \\ -\frac{a_1^2 u_1}{\alpha_1} & -\frac{a_1^2 u_1}{r_1} & 0 & \frac{a_1^2}{r_1\alpha_1} & 0 & 0 & 0 & 0 & 0 \\ 0 & 0 & 0 & 0 & 0 & 0 & 0 & 0 & 0 \\ -\frac{u_2}{\alpha_2} & 0 & 0 & 0 & 0 & \frac{u_2}{r_2} & 0 & -\frac{1}{r_2\alpha_2} & 0 \\ \pi_I - \pi_2 & 0 & 0 & 0 & 0 & -\frac{\alpha_2\pi_2}{r_2} & 0 & 0 & \frac{\alpha_2}{r_2} \\ \frac{a_2^2 u_2}{\alpha_2} & 0 & 0 & 0 & 0 & -\frac{a_2^2 u_2}{r_2} & 0 & \frac{a_2^2}{r_2\alpha_2} & 0 \end{pmatrix} \tag{39}$$

where $W = (\alpha_1, r_1, r_1\tau_1, r_1\alpha_1 u_1, r_1\pi_1, r_2, r_2\tau_2, r_2\alpha_2 u_2, r_2\pi_2)$.

The eigenvalues of the matrix A are $\left\{-\frac{a_1}{r_1}, -\frac{a_2}{r_2}, 0, \frac{a_2}{r_2}, \frac{a_1}{r_1}\right\}$. We give a basis of right eigenvectors of A in the case $\pi_I = \pi_1$ for the sake of simplicity:

- $r_0^{(1)} = (0, 0, 1, 0, 0, 0, 0, 0, 0)$
- $r_0^{(2)} = \left(0, \frac{1}{\pi_1}, 0, \frac{\alpha_1 u_1}{\pi_1}, 1, 0, 0, 0, 0\right)$
- $r_0^{(3)} = (0, 0, 0, 0, 0, 0, 1, 0, 0)$
- $r_0^{(4)} = \left(\frac{1}{r_2 u_2}\frac{\pi_2}{\pi_1 - 2\pi_2}, 0, 0, \frac{1}{r_2 u_2}\frac{\pi_2 r_1 u_1}{\pi_1 - 2\pi_2}, 0, \frac{1}{\alpha_2 u_2}\frac{\pi_1 - \pi_2}{\pi_1 - 2\pi_2}, 0, 1, 0\right)$
- $r_0^{(5)} = \left(-\frac{1}{r_2}\frac{\alpha_2}{\pi_1 - 2\pi_2}, 0, 0, -\frac{1}{r_2}\frac{\alpha_2 r_1 u_1}{\pi_1 - 2\pi_2}, 0, -\frac{1}{\pi_1 - 2\pi_2}, 0, 0, 1\right)$
- $r_{\pm\frac{a_1}{r_1}} = \left(0, 0, -\frac{1}{a_1^2}, \pm\frac{\alpha_1}{a_1}, 1, 0, 0, 0, 0\right)$
- $r_{\pm\frac{a_2}{r_2}} = \left(0, 0, 0, 0, 0, 0, -\frac{1}{a_2^2}, \pm\frac{\alpha_2}{a_2}, 1\right)$

where $r_0^{(1)}$, $r_0^{(2)}$, $r_0^{(3)}$, $r_0^{(4)}$ and $r_0^{(5)}$ are associated with eigenvalue 0 of multiplicity 5. $r_{\pm\frac{a_1}{r_1}}$ is associated with $\pm\frac{a_1}{r_1}$ and $r_{\pm\frac{a_2}{r_2}}$ with $\pm\frac{a_2}{r_2}$. The system (39) is thus hyperbolic. All the characteristic fields of (39) are linearly degenerate.

B. Riemann problem for the stationary contact discontinuity

In this section, we give a procedure to initialize a test case with a stationary contact discontinuity. We recall the Riemann invariants associated to the u_I contact discontinuity of the barotropic Baer Nunziato model:

$$u_I = u_2, \quad m_1(u_2-u_1), \quad m_1(u_2-u_1)^2 + \alpha_1 p_1 + \alpha_2 p_2, \quad \frac{(u_2-u_1)^2}{2} + e_1 + \frac{p_1}{\rho_1}, \tag{40}$$

where we recall that e_1 verifies: $\mathrm{d}e_1/\mathrm{d}\rho_1 = p_1/\rho_1^2$.
We denote $[\![X]\!] = X_R - X_L$, the jump accross an interface where X_R and X_L are the right and left states. Hence we have the following set of jump relations:

$$[\![m_1 u_1]\!] = 0, \tag{41}$$

$$[\![m_1 u_1^2 + \sum_k \alpha_k p_k]\!] = 0, \tag{42}$$

$$[\![\frac{u_1^2}{2} + e_1 + \frac{p_1}{\rho_1}]\!] = 0. \tag{43}$$

From (41), we denote $\overline{m_1 u_1}$ such that: $\overline{m_1 u_1} = (m_1 u_1)_L = (m_1 u_1)_R$. From (43), we obtain:

$$\overline{m_1 u_1}^2 [\![\frac{1}{2\rho_1^2\alpha_1^2}]\!] + [\![e_1 + \frac{p_1}{\rho_1}]\!] = 0. \tag{44}$$

We seek to define a test case where the initial condition is a stationary contact discontinuity. From given jumps $[\![\alpha_1]\!]$ and $[\![\rho_1]\!]$, we deduce the jumps $[\![\frac{1}{2\rho_1^2\alpha_1^2}]\!]$ and $[\![e_1 + \frac{p_1}{\rho_1}]\!]$. Assuming $\overline{m_1 u_1}$ is positive, we can compute its expression from (44). Starting from (42) and a given state $(p_2)_R$, we can deduce the left state $(p_2)_L$ with the following equation:

$$[\![m_1 u_1^2]\!] + [\![\alpha_1 p_1]\!] + (\alpha_2)_R (p_2)_R = (\alpha_2)_L (p_2)_L.$$

References

[1] A. Ambroso, C. Chalons, F. Coquel, and T. Galié. Relaxation and numerical approximation of a two-fluid two-pressure diphasic model. *ESAIM: Mathematical Modelling and Numerical Analysis - Modélisation Mathématique et Analyse Numérique*, 43(6):1063–1097, 2009.

[2] N. Andrianov and G. Warnecke. The Riemann problem for the Baer-Nuziato two-phase flow model. *Journal of Computational Physics*, 195:434–464, 2004.

[3] M.R. Baer and J.W. Nunziato. A two-phase mixture theory for the deflagration-to-detonation transition (DDT) in reactive granular materials. *International Journal of Multiphase Flow*, 12(6):861–889, 1986.

[4] F. Bouchut. On zero pressure gas dynamics. *Series on Advances in Mathematics for Applied Sciences, World Scientific*, 22:171–190, 1994.

[5] F. Bouchut and F. James. Duality solutions for pressureless gases, monotone scalar conservation laws, and uniqueness. *Communications in Partial Differential Equations*, 24:2173–2189, 1999.

[6] C. Chalons, F. Coquel, S. Kokh, and N. Spillane. Large Time-Step Numerical Scheme for the Seven-Equation Model of Compressible Two-Phase Flows. In *Finite Volumes for Complex Applications VI in Springer Proceedings in Mathematics, volume 4*, pages 225–233, 2011.

[7] C. Chalons and J-F Coulombel. Relaxation approximation of the Euler equations. *Journal of Mathematical Analysis and Applications*, 348(2):872–893, 2008.

[8] C. Chalons, M. Girardin, and S. Kokh. Large time step and asymptotic preserving numerical schemes for the gas dynamics equations with source terms. *SIAM Journal on Scientific Computing*, 35(6):A2874–A2902, 2013.
[9] C. Chalons, M. Girardin, and S. Kokh. An all-regime Lagrange-Projection like scheme for 2D homogeneous models for two-phase flows on unstructured meshes. *Journal of Computational Physics*, 335:885–904, 2017.
[10] C. Chalons, P. Kestener, S. Kokh, and M. Stauffert. A large time-step and well-balanced Lagrange-Projection type scheme for the shallow-water equations. *Communications in Mathematical Sciences*, 15(3):765–788, 2017.
[11] F. Chen. *Modélisation d'un jet de gaz dans le collecteur sodium des échangeurs à plaques compacts sodium gaz des réacteurs nucléaires de la filière RNR-Na*. PhD thesis, Aix-Marseille Univ., 2019. `https://www.theses.fr/2019AIXM0380`.
[12] F. Coquel, T. Gallouet, J-M Hérard, and N. Seguin. Closure laws for two-fluid two-pressure models. *Comptes Rendus Mathematique*, 334:927–932, 2002.
[13] F. Coquel, E. Godlewski, and N. Seguin. Relaxation of fluid systems. *Mathematical Models and Methods in Applied Sciences*, 22(8):52, 2012.
[14] F. Coquel, J-M Hérard, and K. Saleh. A positive and entropy-satisfying finite volume scheme for the Baer-Nunziato model. *Journal of Computational Physics*, 330:401–435, 2017.
[15] F. Coquel, J-M Hérard, K. Saleh, and N. Seguin. A robust entropy-satisfying finite volume scheme for the isentropic Baer-Nunziato model. *ESAIM: Mathematical Modelling and Numerical Analysis - Modélisation Mathématique et Analyse Numérique*, 48(1):165–206, 2014.
[16] F. Coquel, J-M Hérard, and K. Saleh. A splitting method for the isentropic Baer-Nunziato two-phase flow model. *ESAIM Proceedings*, 38:241–256, 2013.
[17] F. Coquel, Q. Nguyen, M. Postel, and Q.-H. Tran. Entropy-satisfying relaxation method with large time-steps for Euler IBVPs. *Math. Comput.*, 79:1493–1533, 2010.
[18] B. M. Devassy, C. Habchi, and E. Daniel. Atomization modelling of liquid jets using a two-surface-density approach. *Atomization and Sprays*, 25(1):47–80, 2015.
[19] T. Gallouët, J-M Hérard, and N. Seguin. Numerical modeling of two-phase flows using the two-fluid two-pressure approach. *Mathematical Models and Methods in Applied Sciences*, 14(05):663–700, 2004.
[20] S. Gavrilyuk and R. Saurel. Mathematical and numerical modeling of two-phase compressible flows with micro-inertia. *J. Comput. Phys.*, 175:326–360, 2002.
[21] J. Glimm, D. Saltz, and D. H. Sharp. Two-phase modelling of a fluid mixing layer. *Journal of Fluid Mechanics*, 378:119–143, 1999.
[22] V. Guillemaud. Modelling and numerical simulation of strongly unbalanced two-phase flows. In *18th AIAA Computational Fluid Dynamics Conference*. American Institute of Aeronautics and Astronautics, 2007. `doi.org/10.2514/6.2007-382`.
[23] H. Lochon, F. Daude, P. Galon, and J.-M. Hérard. Computation of fast depressurization of water using a two-fluid model: Revisiting Bilicki modelling of mass transfer. *Computers and Fluids*, 156:162–174, 2017.
[24] S. Peluchon, G. Gallice, and L. Mieussens. A robust implicit-explicit acoustic-transport splitting scheme for two-phase flows. *Journal of Computational Physics*, 339:328–355, 2017.
[25] R. Saurel and R. Abgrall. A multiphase Godunov method for compressible multifluid and multiphase flows. *Journal of Computational Physics*, 150(2):425–467, 1999.
[26] D. W. Schwendeman, C. W. Wahle, and A. K. Kapila. The Riemann problem and a high-resolution Godunov method for a model of compressible two-phase flow. *J. Comput. Phys.*, 212(2):490–526, 2006.
[27] I. Suliciu. On the thermodynamics of rate-type fluids and phase transitions. I. Rate-type fluids. *International Journal of Engineering Science*, 36(9):921–947, 1998.
[28] L. Tallois, S. Peluchon, and P. Villedieu. A second-order extension of a robust implicit-explicit acoustic-transport splitting scheme for two-phase flows. *Computers & Fluids*, 244:105531, 2022.
[29] S. Tokareva and E. Toro. HLLC-type Riemann solver for the Baer–Nunziato equations of compressible two-phase flow. *Journal of Computational Physics*, 229:3573–3604, 2010.
[30] Z. Zou, N. Grenier, S. Kokh, C. Tenaud, and E. Audit. Compressible solver for two-phase flows with sharp interface and capillary effects preserving accuracy in the low Mach regime. *Journal of Computational Physics*, 448:110735, 2022.